Self-assembling Ultrashort NSAID-Peptide Nanosponges: Multifunctional Antimicrobial and Anti-inflammatory Materials

A. P. McCloskey,[a] S. M. Gilmore,[a] J. Zhou,[b] E. R. Draper,[c] S. Porter,[a] B. F. Gilmore,[a] Bing Xu[b] and G. Laverty,*[a]

[a]*School of Pharmacy, Queen's University, Belfast, BT9 7BL, N. Ireland.*

[b]*Department of Chemistry, Brandeis University, Waltham, Massachusetts, MA 02454, USA.*

[c]*Department of Chemistry, University of Liverpool, Liverpool, L69 7ZD, UK.*.

Abstract

Peptide-based materials are receiving significant attention for use within biomedicine due to their high chemical and functional versatility enabling tailoring of their structure to replicate the properties of host tissue and the extracellular matrix. This paper studies the design, synthesis and characterization of NSAID-peptide conjugates. Attachment of NSAIDs to a diphenylalanine-dilysine (FFKK-OH) peptide sequence generates supramolecular hydrogel forming molecules with antimicrobial and anti-inflammatory properties. NSAID-peptides demonstrate broad-spectrum antimicrobial activity against both Gram-positive and Gram-negative bacteria implicated in a variety of antimicrobial resistant nosocomial infections including *Staphylococcus aureus* and *Pseudomonas aeruginosa*. Naproxen-peptides show particular promise, forming biocompatible nanofibrous viscoelastic hydrogel nanosponges composed of β-sheet secondary structures at low concentrations (0.4% w/v). Conjugation of the peptide motif FFKK-OH to naproxen increases selectivity for COX-2 enzyme, implicated in chronic wound scar-tissue formation. Our findings suggest that ultrashort NSAID-peptides have potential use as multifunctional materials for a range of biomedical applications. This includes as topical agents for treatment of chronic wounds, where a profile of persistent inflammation, pain and the presence of infection has been proven to be detrimental to

successful wound repair. This work may also serve as a template for the design of future medical device coatings with tailored antimicrobial and anti-inflammatory properties.

Introduction

Antimicrobial resistance is becoming an increasingly menacing threat to society and is currently attributed to at least 700,000 deaths worldwide annually. A U.K Government review in 2014 concluded that without significant investment in new therapies this total would increase to more than 10 million deaths by 2050, a figure greater than predicted for cancer.[1] Hospital-acquired infections, especially those related to implantation of medical devices and skin wounds, are major contributors to this threat demonstrating an increased prevalence of microorganisms that display resistance to standardly employed antimicrobial therapies. These are responsible for increased patient morbidity and mortality, and significant economic cost due to extended hospital stay/sick days. Infections are particularly problematic among those with increased susceptibility and compromised immunity, for example the elderly and those with under-lying disease.

Wound infections can be categorized into a variety of forms; most problematic being surgical site infections (SSIs), diabetic ulcers and major trauma, for example burns. SSIs are one of the most frequently reported hospital acquired infections accounting for 31% of nosocomial infections and are a reservoir for so-called hospital superbugs including *Staphylococcus aureus* and *Pseudomonas aeruginosa*.[2] SSIs are present in nearly 5% of patients who undergo a surgical procedure and over a third of postoperative deaths are related to SSIs.[3] It is clear SSIs remain a significant burden to healthcare. Failure of antimicrobial therapy and/or unresolved healing can result in the development of a chronic wound.

Chronic infected wounds are particularly problematic with a profile of exaggerated inflammation and resistant infection severely limiting wound healing.[4] They are responsible

for multiple treatment failures and commonly require a minimum of eight weeks to fully resolve, due to increased microbial resistance to standard drug regimens and impaired healing. Nonhealing wounds costs the US healthcare system $3billion annually and affects over 2% of the population. [5,6] Acute and chronic wounds are resolved through similar biomolecular pathways, however chronic wounds commonly stall in the inflammatory phase partly due to the presence of pathogenic biofilm infection.[7] Implanted biomaterials are also associated with an exaggerated host immune response, termed the foreign body response. Sustained inflammation, present primarily within chronic wounds and biomaterial infections, has been proven to be detrimental to wound repair.[8] This has commonly been minimized and controlled using steroidal and non-steroidal anti-inflammatory drugs (NSAIDs), limiting the action of inflammatory mediators such as prostaglandins. Long-term systemic use of such drugs leads to undesirable side effects including adverse gastrointestinal, renal and cardiovascular risks. Debate still exists regarding the use of systemic NSAIDs to aid wound repair due to possible anti-proliferative effects demonstrated in animal studies and their possible contribution to increasing the severity of group A streptococcal infections.[9,10] Despite reservations with systemic NSAID use, localized sustained release systems are commonly employed and NSAID topical applications demonstrate benefit in the treatment of chronic wounds.[11] For example an ibuprofen foam formulation provides localized delivery, reduced pain, a moist environment and has been proven to be advantageous for the resolution of chronic venous leg ulcers.[12]

There has been increased interest in the therapeutic potential of antimicrobial peptides. Displaying multiple modes of intracellular and extracellular action, antimicrobial peptides demonstrate a reduced propensity for developing antimicrobial resistance and are a significant prospect for solving the current shortage of antimicrobials in pharmaceutical development.[13] Several research groups have studied their incorporation into synthetic hydrogel matrices for

the prevention of biomaterial and wound infections with promising results thus far.[14-16] Hydrogels possessing inherent antimicrobial properties represent a significant benefit by reducing microbial contamination within the matrix and at the wound/implantation site.[17] Self-assembling biomimetic hydrogels, including peptide-based strategies, have received attention as biofunctional materials and drug delivery platforms due to their similarity to the extracellular tissue matrix. Peptide-based materials possess: increased chemical functionality and versatility; improved biocompatibility; increased water capacity; moisture vapor transmission and gaseous exchange; biodegradability and tailored immunogenicity. Hydrogels provide improved healing at wound sites by enabling rapid absorption of wound exudate and protection of newly formed skin. Researchers have begun to employ a strategy whereby peptides are optimized to obtain multi-functionality, both pharmacological (antimicrobial, anti-biofilm, anti-inflammatory, analgesia) and physical (self-assembly, hydrogelation), within a single molecule. Most recently our group developed an ultrashort cationic peptide motif with selective activity against resistant pathogens implicated in medical device related infections.[18] Ultrashort peptides are of particular interest to the pharmaceutical industry as they are generally more cost-effective to synthesize relative to their larger peptide/protein counterparts and therefore more realistic molecules for clinical translation.

Self-assembling hydrogel systems based on drug molecules eliminates the necessity for a drug delivery vehicle, typically a synthetic polymer and may be tailored to respond to environmental and physiological stimuli, for example pH change or the presence of specific enzymes.[19,20] Synthetic-based polymers demonstrate limited drug loading, are difficult to functionalize and acidic degradation products can induce an unwanted inflammatory response.[21] The presence of aromatic groups, such as those present within NSAIDs, facilitates assembly of NSAID-peptide conjugates where the NSAID moiety replaces more traditional aromatic groups found in self-assembling systems such as carboxybenzyl,[22] 9-

fluorenylmethyloxycarbonyl (Fmoc),[23] and 2-naphthoyl (Nap).[24] Work thus far has focused on NSAIDs clinically used as topical preparations for acute pain, for example ibuprofen and naproxen.[25] Recently a multifunctional approach has been successful in creating an anti-inflammatory and anti-HIV hydrogel using naproxen conjugated to reverse transcriptase inhibitors via a peptide linker. [26] The idea of a multifunctional antimicrobial and anti-inflammatory platform is adopted from nature where herb extracts curcumin (*Curuma longa*), dayflower (*Commelina diffusa*) and bark (*Spathodea campanulata*) have demonstrated benefit in wound healing.[27,28] Building on previously investigated NSAID conjugated peptides and antimicrobial peptides we have developed novel self-assembling NSAID-peptides utilizing racemic (±)-ibuprofen (Ibu), indomethacin (Ind) and (S)-(+)-naproxen (Npx) (Fig. 1).
This report examines the synthesis and characterization of NSAID conjugated ultrashort cationic self-assembled peptide hydrogels as potential antimicrobial and anti-inflammatory biomaterials. Incorporation of an NSAID into the ultrashort carboxylic acid terminated motif (FFKK-OH) was hypothesized to confer improved hydrogel strength and cyclooxygenase (COX) inhibitory properties to the molecule. The development of a NSAID conjugated hydrogelator may also serve as a carrier for other therapeutic agents since the arrest of the inflammatory response is one of the most important factors in successful application of biomaterials.[29]

Experimental methods

Materials

Wang resin preloaded with Fmoc-Lys(Boc) (mesh size 100-200, 0.65 mmol/g substitution), (2-(1H-benzotriazol-1-yl)-1,1,3,3-tetramethyluronium hexafluorophosphate) (HBTU), diisopropyl ethylamine (DIEA), Fmoc and Boc protected amino acids were obtained from Novabiochem, Merck KGaA (Dramstadt, Germany). 37% hydrochloric acid (HCl), sodium

hydroxide anhydrous pellets (≥99%), acetonitrile (HPLC grade, ≥99.93%), (±)-ibuprofen (≥98%), indomethacin (≥99%), (S)-(+)-naproxen (≥99%), deuterated dimethyl sulfoxide (d_6-DMSO), deuterium oxide (D_2O), deuterium chloride (DCl), sodium deuteroxide (NaOD), trifluoracetic acid, triisopropylsilane, thioanisole and Whatman pH indicator paper (pH 1-14) were purchased from Sigma-Aldrich (Dorset, U.K.). NCTC Clone 929 (ATCC CCL 1) murine fibroblast subcutaneous connective tissue cells, *S. epidermidis* (ATCC 25984), *S. aureus* (ATCC 6584), *P. aeruginosa* (PAO1) and *E. coli* (ATCC 11303) supplied by LGC Standards (London, U.K). AlamarBlue® was obtained from AbD Serotec (Oxford, U.K.). Sterile Nunc™ 96-well microtiter plates supplied by VWR International (Leicestershire, U.K.). Fresh defibrinated equine erythrocytes were purchased from Laboratory Supplies and Instruments Ltd (Antrim, U.K.). Cayman's COX fluorescent inhibitor screening assay kit was obtained from Cambridge Bioscience Ltd (Cambridge, U.K.).

Synthesis, purification and identification

NSAID-peptide hybrids (IbuFFKK, IndFFKK and NpxFFKK) were synthesized as per standard Fmoc-based solid-phase peptide methods using a nitrogen bubbler apparatus.[18] Wang resin preloaded with Fmoc-Lys(Boc) was utilized to produce carboxylic acid terminated peptides, upon cleavage with 95% v/v trifluoracetic acid, 2.5% v/v triisopropylsilane and 2.5% v/v thioanisole for 3 hours at room temperature. The peptide amine terminus was conjugated to the corresponding carboxylic acid of the NSAID before cleavage. Standard HBTU coupling was performed in dimethylformamide (DMF) with 4-fold molar excess of DIEA and 3-fold excess of Fmoc-protected amino acid or NSAID used for coupling for 3 hours at room temperature. Precipitation was achieved using cold diethyl ether (-20 °C). Crude product was dissolved in ethyl acetate and subjected to a series of washes with 1 mM HCl (3 x 50 ml) and water (3 x 50 ml and dried over anhydrous magnesium sulfate ($MgSO_4$).

NSAID-peptide identities were confirmed using ^{1}H NMR analysis (Varian Unity Inova 400 spectrometer, Varian systems, Palo Alto, California, U.S.A.) in d_6-DMSO and electrospray mass spectroscopy (Thermo Finnigan LCQ Deca ion trap, Thermo Fisher Scientific, Waltham, Massachusetts, U.S.A.). NSAID-peptide purity was determined by reverse-phase-HPLC (Agilent 1260 series, Agilent Technologies Ltd, Cork, Ireland), using a Gemini C18 column (250 mm x 4.6 mm) with a flow rate of 1.5 mL/min and gradient of 2-60% acetonitrile (30 minutes) in 0.05% TFA-water. All NSAID-peptides were found to have purity greater than 95%.

Self-assembling pH-triggered gelation

NSAID-peptide hydrogels prepared by a process of pH-triggered induction.[18] The method of gelation followed the sequence of steps outlined for of 2% w/v NSAID-peptide formulations in Table 1. A stock solution was prepared by suspending each NSAID-peptide in deionized water. Complete dissolution was achieved at pH 9 via titration with 1 M NaOH due to deprotonation of the terminal carboxylic acid moiety. Changes in pH were monitored using Whatman pH paper. Protonation of the terminal carboxylate ion, by titration with 0.5 M HCl to pH 7, enabled formation of homogeneous hydrogels at concentrations above the minimum gelation concentration (% w/v) for each molecule. Minimum gelation concentration (% w/v) was defined as the lowest concentration of NSAID-peptide that formed a self-supporting hydrogel, observed via a gel inversion assay after 24 hours development.[30] Gels and solutions were differentiated based on flow characteristics with gels remaining suspended and solutions demonstrating flow.

Table 1 Stepwise formulation of a self-assembling pH-triggered 2% w/v NSAID-peptide (500 µL)

Formulation step	Constituent [a)]	Quantity
1	NSAID-peptide	10mg pre-weighed
2	Deionized H_2O or D_2O	200 µL (in 50 µL aliquots)
3	1M NaOH or NaOD	50 µL (in 10 µL aliquots)
4	Deionized H_2O or D_2O	200 µL (in 50 µL aliquots)
5	0.5M HCl or DCl	20 µL (in 10 µL aliquots)
6	Deionized H_2O or D_2O	to 500 µL

[a)] Deuterated solvents employed for FTIR purposes and IbuFFKK where relevant in text

Cryo-scanning electron and transmission electron microscopy

NSAID-peptides were prepared via pH induction as described and analyzed for 3D morphology using a Hitachi Analytical Benchtop SEM TM3030 (Hitachi High-Technologies Europe, Berkshire, U.K.) with Deben Cool Stage (Deben, Suffolk, U.K.). Cryo-SEM samples were freeze-dried by vacuum lyophilization at 2 °C. Images were obtained at -10 °C, using an accelerating voltage of 15 kV and a range of magnifications (15-30 000x).[31] TEM was performed using a FEI Morgagni 268 transmission electron microscope (FEI electronics, Burlington, Massachusetts, U.S.A.). A negative staining technique was employed.[31] TEM samples were placed on 400 mesh copper grids, glow discharged and coated with a carbon film (35nm), rinsed thrice with double distilled water, then stained trice with a 2% w/v solution of uranyl acetate. Excess stain was removed by blotting with filter paper. The grids were left to air dry prior to examination of the 3D architecture of the NSAID-peptide samples.

Fourier transform infrared spectroscopy

FTIR spectra were obtained at a resolution of 2 cm^{-1} and over wavelengths 4000-400 cm^{-1} (128 scans) using a Jasco 4000 series FTIR spectrometer (Jasco Inc. Tokyo, Japan). Samples were prepared as described above but using deuterated solvents (D_2O, DCl, NaOD). Hydrogels were sandwiched between two calcium fluoride discs (0.05 mm spacer). A D_2O, DCl, NaOD mixture, prepared to the same concentrations as NSAID-peptide containing samples, was used as a background and subtracted from all spectra.

Oscillatory rheology

Dynamic rheological measurements were performed using an Anton Paar Physica MCR301 rheometer. A cup and vane measuring system was used to perform frequency sweeps. For frequency 2 mL of the gels were prepared in 7 mL Sterilin vials as described previously.[30] All experiments were performed at 25 °C from 1-100 rad s^{-1} at a strain of 0.0003 %.

Bacterial susceptibility assay

The ability of NSAID-peptides to reduce bacterial viability were tested using a colony counting method previously outlined by Mateescu and Jiang.[32,33] *S. epidermidis* (ATCC 25984), *S. aureus* (ATCC 6584), *P. aeruginosa* (PAO1) and *E. coli* (ATCC 11303) were subcultured for 24 hours at 37 °C in Müller Hinton broth (MHB), optically adjusted to an optical density reading of 0.3 at 550 nm (1×10^8 colony forming units per milliter (CFU/mL)) in phosphate buffered saline (PBS) and further diluted in MHB (equivalent to 2×10^6 CFU/mL) prior to plating 100 μL into each well of a microtiter plate containing 100 μL of self-assembled NSAID-peptide (2-0.5% w/v) prepared as described above. Control wells included bacteria treated with PBS, as the negative control (100% survival) and 2% w/v HPMC as an inert hydrogel to study the effect of gelation on bacterial viability. Inoculated

microtiter plates were incubated for 24 hours in a Gallenkamp gyrorotary incubator (37 °C) and 20 µL samples were taken from each well, serially diluted in PBS and transferred onto Müller Hinton agar plates for colony counting via the Miles and Misra method. Results were displayed as the mean (Log_{10} CFU/mL) of four replicates.

Cyclooxygenase enzyme inhibition assay

The anti-inflammatory activity of the NSAID-peptides (1- 2000 µM) were determined against both COX-1 and COX-2 enzymes using a COX Fluorescent Inhibitor Screening Assay Kit. Reagents used were supplied and prepared according to the kit protocol. Potassium hydroxide (KOH), DMSO, COX-1 (SC-560) and COX-2 (DuP-697) inhibitors were supplied ready for use. Assay buffer (x10) (final formulation: 100 mM Tris-HCl, pH 8.0), heme, arachadonic acid (final concentration: 2 mM) were prepared as per kit instructions. The test plates (one plate per COX enzyme) were set up according to the kit protocol with triplicates for each NSAID-peptide concentration. The inhibitor/sample was incubated with the enzyme for 5 minutes at room temperature. 10 µL of 10-acetyl-3, 7-dihydroxyphenoxazine (ADHP) was added followed by 10 µL of arachidonic acid (reaction initiator). The plates were incubated for 2 minutes at room temperature and then read at an excitation wavelength of 530 nm and an emission wavelength of 585 nm using a FLUOstar Omega Fluorometer (BMG Labtech, Ortenberg, Germany) and Gen5 data analysis software (BioTek, Swindon, U.K.). IC_{50} (concentration needed to inhibit COX activity by half) values were interpreted from activity curves (Log_{10} inhibitor vs normalized response) using GraphPad Prism 6 (GraphPad Software Inc, California, USA). The percentage inhibition of the COX enzymes was calculated by measurement of respective emission wavelengths (585nm) and using Equation 1.

% COX inhibition = (COX activity no inhibitor – NSAID/peptide activity)/(COX activity no inhibitor) x 100

(1)

In each case, the background fluorescence was subtracted from each fluorescence value obtained. The percentage inhibition of the test inhibitors SC-560 and DuP-697 enabled a direct comparison to be made between the NSAID-peptide activity and that of a known inhibitor. NSAID only wells ((±)-ibuprofen, indomethacin, (S)-(+)-naproxen: 1-50 μM) were tested to determine whether or not conjugation of the NSAID to the peptide altered anti-inflammatory activity/selectivity. All compounds were assayed in triplicate.

Hemolysis assay

The ability of NSAID-peptides to induce hemogolobin release from fresh equine erythrocytes was tested using a method previously outlined by our group.[34] 100 μL of equine erythrocytes were treated with 100 μL of NSAID-peptides for 1 hour at 37 °C. Control wells included 0.1% v/v Triton X-100 (100% hemolysis, positive control) and PBS (0% hemolysis, negative control). Following incubation the erythrocytes were centrifuged at 1000 *g* and aliquots of the supernatant used to determine hemoglobin released in a fresh 96-well microtiter plate read at 405 nm using a Tecan Sunrise plate reader (Tecan UK Ltd, Reading, U.K.) and Equation 2 below. Results are reported as the mean of six replicates.

% hemolysis = (Abs_{405nm} peptide – Abs_{405nm} PBS)/(Abs_{405nm} 0.1% triton X - Abs_{405nm} PBS) x 100

(2)

Cell Viability Assay

Cell cytotoxicity was assessed using murine fibroblast subcutaneous connective tissue NCTC clone 929 (ATCC CCL 1). Cells were cultured in Minimum Essential Medium (MEM) containing phenol red with Earle's Salts and L-glutamine, supplemented with 10% horse serum and 1% penicillin and streptomycin (Invitrogen, Paisley, U.K.). Cells were grown at 37 °C and 5% CO_2 and subcultured at 80-90% confluency. Subculturing involved removal of spent media, washing with sterile PBS and detachment of cell monolayers with 0.05% trypsin/ 0.53 mM EDTA.4Na solution (Invitrogen, Paisley, U.K.). Cells were cultured until at least third passage and inoculated at 1 x 10^4 cells per well in 96-well microtiter plate and incubated for 24 hours. The media was then removed and the cells exposed to 100 µL of a range of NSAID-peptide samples for 24 hours. Control wells included PBS (100% viability, negative control) and 70% ethanol treated cells (100% kill, positive control). Following exposure to NSAID-peptides, cell viability was assessed using a 10% v/v solution of alamarBlue® diluted in supplemented MEM and allowed to develop for 10 hours. Absorption was measured at 570 nm using a Tecan Sunrise plate reader. Cell viability was calculated using Equation 3 below and reported as the mean of six replicates.

$$\% \text{ cell viability} = 100 - [(Abs_{570nm} \text{ peptide} - Abs_{570nm} \text{ PBS})/(Abs_{570nm} \text{ 70\% ethanol} - Abs_{570nm} \text{ PBS}) \times 100] \quad (3)$$

Cell cytotoxicity was also analysed using a Cytotoxicity Detection Kit^{PLUS} assay (Sigma-Aldrich, Dorset, U.K.) that quantifies lactate dehydrogenase (LDH) release. LDH acts as a marker for toxicity and is rapidly released from the cell cytosol when the plasma membrane is damaged. After 24 hours incubation with NSAID-peptides 100 µL of the prepared Cytotoxicity Detection Kit^{PLUS} test reagent was added to each well and incubated for 5

minutes after which 50 µL of the stop reagent was added to each well and absorbance measured at 490 nm. A high LDL release control, corresponding to 100% toxicity, was created via addition of 5 µL of lysis solution to non-peptide treated wells 15 minutes before the addition of prepared Cytotoxicity Detection Kit^{PLUS} test reagent. Aside from background absorbance reading, three additional experimental controls were used (as per manufacturer's protocol). These were: a) the peptide at the highest concentration used in media alone (500 µM), this is compared to the background to assess possible additional absorbance caused by the treatment; b) media and LDH standard; c) peptide at highest concentration (500 µM) used in media with an equal volume of LDH standard as a control to examine the possible effect of the peptide on an equal quantity of LDH standard (checking if peptide is quenching or enhancing the LDH release). No significant addition or reduction was observed in the absorbance for each of these three controls. Cell viability was calculated using Equation 4 below and reported as the mean of six replicates.

$$\% \text{ toxicity} = (Abs_{490nm} \text{ peptide} - Abs_{490nm} \text{ PBS})/(Abs_{490nm} \text{ High LDL control} - Abs_{490nm} \text{ PBS}) \times 100 \quad (4)$$

A LIVE/DEAD® Viability/Cytotoxicity fluorescent assay (Thermo Fisher Scientific, Waltham, MA, USA) was used to quantify the ratio of viable to non-viable NCTC 929 cells alongside fluorescence microscopy (EVOS FL microscope, Thermo Fisher Scientific, Waltham, MA, USA). Following 24 hours incubation with NSAID-peptides, NCTC 929 cells were incubated for 20 minutes with a mixture of 4 µM ethidium homodimer-1 and 2 µM calcein AM in PBS. Viable cells stained green due to the conversion of calcein AM to calcein, whilst non-viable cells stained red due to ethidium homodimer-1. Three randomly chosen areas were selected for quantitative analysis with 200 cells counted for the presence of viable and non-viable cells.

Statistical analysis

Statistical analyses were performed using Microsoft Excel 2013 and GraphPad Prism 6. Standard deviations were obtained at each concentration of NSAID-peptide tested based on six replicates for quantitative bacterial viability assays and mean values obtained. For cell cytotoxicity assays standard deviations and mean values were also obtained from six replicates at each concentration. Statistical analyses were employed using a Kruskal-Wallis test, with a Dunn's multiple comparisons test used to identify individual differences between the reduction in bacterial viability for each NSAID-peptide hydrogel relative to the negative PBS control. A Kruskal-Wallis test, followed by a Dunn's multiple comparisons test, was also utilized for statistical analysis of tissue culture cytotoxicity data by comparison of percentage viability (alamarBlue®) and toxicity (LDH assay) for the NSAID-peptides employed to the PBS negative control (100% viability). Hemolysis data was compared by the same statistical method with percentage hemolysis compared to the PBS, negative, non-hemolytic, control (0% hemolysis). Non-parametric Kruskal-Wallis tests were employed rather than parametric Analysis of Variance (ANOVA) as data was shown to be non-normally distributed using the Kolmogorov and Smirnov method. In all cases a probability of $p < 0.05$ denoted significance.

Results and discussion

Gel inversion assay

A variety of methods exist to successfully induce peptide hydrogelation including pH, thermal (heat-cool) and enzymatic means. In order to ensure the conditions that mediate hydrogelation were replicated as closely as possible we decided to utilize a pH-triggered approach, to a final physiological pH of 7.4, at room temperature and using L-amino acid isomers. Diastereoisomers of NSAID peptides have previously demonstrated different behavior in relation to self-assembly and hydrogelation.[25] All NSAID-peptides formed clear solutions at

pH 9 and above. Hydrogelation is driven by subsequent titration of acid, highlighting the role of the terminal carboxylic acid moiety in self-assembly. [18]

To enable hydrogelation a critical balance is required between molecular hydrophilicity and hydrophobicity with the surrounding medium, primarily water, providing excellent capacity for hydrogen bonding.[35,36] NpxFFKK demonstrated the greatest capacity to form stable hydrogels possessing a critical gelation concentration of 0.4% w/v (Table 2, Figs. 2c and S7). IbuFFKK was unable to form hydrogels in standard deionized water (H_2O) instead forming an opaque, white precipitate (Fig. S4). Interestingly IbuFFKK formed a transparent soft gel at 2% w/v using deuterated water (D_2O) (Figs. 2a and S5). This phenomenon may be due to increased hydrogen bond strength between deuterated hydrogen and electron donors (amines, carbonyl and carboxylic acid groups) present within the NSAID-peptide primary structure.[37,38] The number of hydrogen bonds per molecule of water is also higher for deuterated water compared to standard water.[38] As hydrogel formation is a delicate balance between solubilization and precipitation the use of deuterated water may favor increased hydrogen bond formation and improved solubilization for IbuFFKK resulting in formation of a clear hydrogel at 2% w/v. IndFFKK was able to form a self-supporting supramolecular hydrogel at 1.5% w/v (Fig. S6) becoming an increasingly white and opaque hydrogel as the concentration increased to 2% w/v (Fig. 2b).

Table 2 Critical gelation concentrations (% w/v) for each NSAID-peptide

NSAID-peptide	Critical gelation concentration (% w/v)
IbuFFKK	2 [a)]
IndFFKK	1.5
NpxFFKK	0.4

[a)] Deuterated solvents employed

Microscopy

Transmission electron microscopy (TEM) and cryogenic scanning electron microscopy (cryo-SEM) were utilized to examine the nanoscale architecture of the molecular assemblies. NpxFFKK hydrogels were found to be composed of nanofibers that entangled to form an entangled network (Figs. 3c and S8c and S10c). Naproxen has previously demonstrated ability to self-assemble into supramolecular hydrogels with nanofibrous architecture when attached to a variety of peptidomimetic molecules including peptide amphiphiles and β-peptides.[21,39] By contrast 2% w/v IbuFFKK forms less uniform, non-fibrous structures in the presence of deuterated water (Figs. 3a and S8a and S10a). Interactions between these nanoparticles and the surrounding solvent are sufficient to form a self-supporting supramolecular hydrogel as defined by the vial inversion assay.[30] However rheological analysis, detailed below, confirms that the resulting material more closely resemble a viscous liquid with surfactant-like properties. Cryo-SEM images for 2% w/v IbuFFKK in standard deionized water show the presence of a non-uniform fibers (Fig. S9a) and particles (Fig. S9b) that result in formation of a white precipitate. IndFFKK formed short nanotape-like structures (Figs. 3b and S8b and S10b) where hydrophobic segments are packed tightly away from the aqueous interface. These appear less uniform, forming areas of dense pockets, compared to the nanofibrous architecture of NpxFFKK. These networks of, varying morphologies, are responsible for the immobilization of surrounding solvent molecules resulting in gel formation. [21] The structural morphologies correlate well to the oscillatory rheological profiles, most notably the storage moduli, as discussed further below.

However, the molecular-level understanding of the exact mechanism of peptide gelation kinetics remains unclear despite extensive research and warrants further investigation within the field.[40] It should also be noted that analysis of TEM images of gels, such as morphology of fibers, may not accurately represent the gel network and so should be done with caution.

TEM images are of dried gels, whereas tests such as rheology are carried out on wet gels. Therefore, the structures observed by SEM could be due to drying effects.[41,42]

Fourier transform infrared spectroscopy

The secondary structures of NSAID-peptide nanostructures were determined by Fourier Transform Infrared (FTIR) spectroscopy. All FTIR studies were conducted in deuterated solvents, acknowledging the difficulty encountered using standard water due to strong absorbance within the amide I region (1700-1600 cm^{-1}).[21] The amide I band is generated through stretching of the C=O bond and its participation in hydrogen bonding provides an insight into peptide secondary structures. All NSAID-peptides were studied at or above critical gelation concentrations (2% w/v). NpxFFKK demonstrated the most predominant β-sheet secondary structure characterized by a strong reduction in transmittance at 1630 cm^{-1} (Fig. S11).[43] This trough is less pronounced for IndFFKK and particularly IbuFFKK owing to less uniform nanoparticle and nanotape structures respectively. However, they both possess a shoulder-like reduction in transmittance at 1679 cm^{-1} possibly linked to the presence of antiparallel β-sheets (Fig. S11). Increased concentration of NpxFFKK, from 0.5 to 2.0% w/v, correlated to a respective reduction in transmittance at 1630 and 1679 cm^{-1} owing to a greater presence of β-sheet secondary structures and more rigid hydrogels at 2% w/v NpxFFKK (Fig. S12). However, interpreting this data for short dipeptide molecules is often difficult as has been seen with other ultrashort peptide hydrogels.

Oscillatory Rheology

Oscillatory rheology was utilized to study the viscoelastic properties of 2% w/v self-assembled NSAID-peptide hydrogels (Fig. 4). The frequency dependence of their storage (G′) and loss moduli (G″) were measured using a dynamic frequency sweep, varying the

oscillation frequency (1-100 rad s^{-1}) at a constant oscillation amplitude (0.0003%) and temperature (25 °C).

NpxFFKK exhibits viscoelastic properties of a solid-like material as observed by the maximal storage modulus (G′: ~398 Pa) being ten times larger than the maximal loss modulus (G″: ~39.8 Pa). They are independent of frequency and demonstrate good tolerance to external shear force. NpxFFKK has the highest mean storage modulus and greatest gel strength of the NSAID-peptides (G′: ~398). Its G′ and G″ are comparable to that of the widely reported FmocFF hydrogels.[44] A larger conjugate system, conferred by the presence of naproxen in NpxFFKK (Fig. 1c), enables stronger π- π and van der Waals' intermolecular interactions between NpxFFKK molecules and allows longer fibers and more entangled arrangement of nanofibers as observed via microscopy (Fig. 3c). Similarly IndFFKK is capable of forming a stable hydrogel at 2% w/v possessing a mean G′ of 25.1 Pa and a mean G″ of 6.6 Pa. Reduced G′ and G″ in comparison to NpxFFKK is explained by formation of shorter nanotape architectures rather than longer nanofiber structures observed in NpxFFKK gels (Figs. 3b and S8b and S10b). Despite forming what appears to be a self-supporting hydrogel upon inversion at a concentration of 2% w/v in deuterated water (Fig. 2a), rheology confirms IbuFFKK does not form a hydrogel with significant mechanical rigidity. A high dependence on frequency shows that it is behaving as a liquid rather than a gel, as gels show no dependence on frequency. This is due to reduced aromatic-aromatic (π- π) interactions provided by the terminal isopropyl-substituted phenyl group of IbuFFKK (Fig. 1a) that are only sufficient to allow formation of non-uniform nanoparticle structures. This result is similar to that observed previously by the Xu group where IbuFF demonstrated a low G′ value of only 13 Pa.[25]

Bacterial Susceptibility

The antibacterial activity of NSAID-peptides was tested using a viable count assay after 24 hour exposure to varying concentrations of NSAID-peptides. Clinically relevant bacterial strains, implicated in a variety of antibiotic resistant nosocomial infections (biomaterial and wounds), were selected, namely: methicillin resistant *S. epidermidis* (ATCC 25984), *S. aureus* (ATCC 6584), *P. aeruginosa* (PAO1) and *E. coli* (ATCC 11303). All NSAID-peptides demonstrated broad-spectrum antibacterial activity (Gram-positive and Gram-negative) (Figs. 5, 6, S13 and S14). The mechanism of action of our NSAID-peptides is likely to follow the key parameters of antimicrobial peptide activity, namely hydrophobic bulk and cationic charge enabling interaction with bacterial membranes.[13] The addition of two units of cationic charge, in this case lysine, to an ultrashort (less than seven amino acid units) peptidomimetic sequence is sufficient to confer antimicrobial activity.[34] As previously demonstrated by our group, the ε-amino group of lysine has the ability to interact with negatively charged bacterial membranes and their anionic hydroxylated phospholipids resulting in detergent-like effects, cell lysis and death.[18]

At least a three Log_{10} CFU/mL (99.9%) reduction in viable bacteria, commonly employed as a threshold for bactericidal efficacy, was observed for each NSAID-peptide at concentrations of 0.5% w/v and above.[45] Statistical analysis, however, shows NpxFFKK to be the only NSAID-peptide that is significantly bactericidal against all four isolates with improved activity correlating to increased concentration. For example, significant bacterial kill was achieved at concentrations of 1.5% w/v and above for Gram-negative *P. aeruginosa* and *E. coli*; 1.0% and above for Gram-positive *S. epidermidis* and 0.5% w/v and above for *S. aureus*. A reduction greater than 5.5 Log_{10} CFU/mL was obtained for 2% w/v NpxFFKK against *S. epidermidis* and *S. aureus*. The improved antimicrobial efficacy of NpxFFKK may be related to its ability to form a viscoelastic hydrogel of uniform nanofibrous architecture. Recent studies have

suggested that that molecular folding, structural conformation, assembly state and bulk mechanical properties are important considerations for the rational design of antimicrobial selective hydrogels.[17,46,47] We propose our NpxFFKK hydrogel acts similarly to the dimethyldecylammonium chitosan-graft-poly(ethylene glycol) methacrylate (DMDC-Q-g-EM) 'anion sponge' developed by the Chan-Park group.[48] Based on this theory, the nanoporous architecture of cationic NpxFFKK allows increased interactions, termed 'suctioning,' with anionic constituents of the bacterial membrane. Therefore the hydrogel acts as a molecular sponge resulting in bacterial membrane disruption and cell death.

The inclusion of cationic charge density within the hydrogel matrix is a key parameter for selective antimicrobial activity as demonstrated by the range of β-hairpin hydrogels (MAX, PEP6R and MARG) developed by the Schneider group.[49,50,51] Hydrogelation alone is not sufficient to bestow antimicrobial activity, for example by restricting the diffusion of chemical messengers and nutrients. This is confirmed by the observed lack of efficacy of non-ionic 2% w/v hydroxypropyl methylcellulose (HPMC) against all bacterial isolates. This is an unsurprising observation given that bacteria commonly prefer to exist and successfully survive within a surface-attached, extracellular polymeric matrix granted by the biofilm phenotype. As the Dong group hypothesized for their multi-domain peptides, the combined effect of localized cationic charge on the hydrogel surface and the porous network of crosslinked nanofibers (Fig. 3c, S8c and S10c) are likely to be responsible for the improved antimicrobial efficacy of NpxFFKK.[32,47] Our ultrashort peptide motif possesses improved antimicrobial efficacy compared to related peptide-based strategies in the literature at a reduced polymer size and increased ease of synthesis.

Chronic wounds fail to heal and are characterized by persistent inflammation due in part to the presence of bacterial biofilms.[52] Research by Wolcott and Rhodes also demonstrated that the presence of bacterial infection in chronic wounds perpetuates a destructive level of

inflammation.[53] Treatments active against resistant bacteria allowed non-healable, chronic wounds to heal. They concluded that topical agents with the ability to disrupt biofilm forming microorganisms should be central to the treatment of chronic wounds.[54] Previous work by our group demonstrates the significant efficacy of the FFKK-OH peptide motif against bacterial isolates. They may have a significant clinical benefit for the treatment of chronic infected wounds.[18] Whilst NSAIDs have recently been demonstrated to possess antibacterial activity alone by specifically targeting DNA Clamp, a key bacterial protein involved in multiplication, its inclusion within our motif is primarily to provide potential anti-inflammatory, analgesic and self-assembly characteristics.[55] The benefits of NSAIDs as antibiotic therapy in their own right have to be verified clinically. Such studies provide hope to extend the currently available antibiotic formulary utilizing a readily available and licensed group of drugs.

These results may inform future strategies whereby the host immune response is controlled in combination with antimicrobial and antibiofilm activity. For example IDR-1018, a synthetic variant of the host defense peptide LL-37, has an ability to inhibit biofilm formation in combination with immunomodulatory effects which prevent tissue damage.[56] Although IDR-1018 did not display an ability to self-assemble into supramolecular structures the Hancock group did demonstrate antibiofilm peptides could be used to control mediators of the immune response, including stimulating monocyte chemoattractant protein (MCP-1) and inhibiting lipopolysaccharide induced interleukin-1β (IL-1β) production in peripheral blood mononuclear cells.[57]

Cyclooxygenase enzyme inhibition

We performed *in vitro* inhibition assays for both COX-1 and COX-2 in the presence of varying concentrations of NSAID-peptides. Molecular modeling, utilizing the crystal structure of COX enzymes, has previously shown that the NSAID carboxylate end is available for

peptide modification due to the large open space in the structure of COX.[46,58] Addition of the peptide sequence FFKK-OH to the NSAID motif increases respective IC_{50} values relative to NSAID only values. However, the NSAID-peptide motifs retain significant inhibitory activity with IC_{50} values within the μM range. For example, NpxFFKK exhibits IC_{50} values of 204.20 μM and 73.47 μM against COX-1 and COX-2 respectively compared with naproxen only values of 13.26 μM (COX-1) and 8.365 μM (COX-2) (Fig. S15). NSAID-peptides also demonstrate increased selectivity for inhibiting COX-2 compared to NSAID alone. Selectivity (S) values, related to the ratio of IC_{50} COX-1: IC_{50} COX-2, are highest for NpxFFKK (S = 2.78) compared to naproxen only (S = 0.19). This correlates to previous work on NSAID-peptide hydrogelators where it was proven that addition of a peptide moiety increased COX-2 selectivity.[25,26] Replacing L-amino acid enantiomers with their respective D-forms may increase inhibition of COX-2 further.[46] Selective COX-2 inhibition is preferred clinically, especially for systemic administration of NSAIDs, due to a reduction in renal and gastrointestinal side effects linked to COX-1 inhibition but may also have potential value in the chronic wound environment.[59] Studies have shown that upon degradation, the pharmaceutical efficacy of NSAIDs in theory should be maintained and pharmacological activity exhibited until the hydrogel has completely degraded. Therefore an extended profile of anti-inflammatory activity should be possible.[60]

COX-2 and its enzymatic product prostaglandin E2 (PGE_2) demonstrate an important role in the early acute host response to stimuli such as wounds and are responsible for the upregulation of inflammatory mediators. Separate studies in murine and rat wound models by Blomme and Futagmi showed a significant induction of COX-2 expression after 12 hours, peaking three days after injury.[61,62] However within chronic wounds, COX-2 has recently been associated with the unwanted development of scar tissue in the latter stages of adult wound repair.[63,64] Therefore NSAID-peptide conjugates with increased selectivity for COX-2

inhibition may be of benefit in the chronic stages of wound healing, replicating fetal wound healing where scarless healing is linked to a reduced inflammatory response.[64] Despite this there is an appreciation that wound healing is a complex pathway and the exact role of multiple inflammatory mediators (cytokines, macrophages, matrix metalloproteinases) has not yet been fully elucidated.[6] In particular, the diverse nature of the immune and inflammatory response to foreign medical implants favors the use of corticosteroids, rather than NSAIDs, due to their broad-spectrum of activity against inflammatory mediators such as leukotrienes.[65] NSAID-peptides may serve a greater purpose within chronic wound healing, providing localized pain relief, antimicrobial and anti-inflammatory activity. Removal of an avascular fibrous capsule that surrounds implanted medical devices may be promoted by inclusion of pro-angiogenic factors including vascular endothelial growth factor (VEGF). Our nanomaterials have the potential to act as a drug delivery platform for the design of future medical device coatings incorporating such factors.[11] The effect of NSAID-peptides nanostructures on mediators of the immune response. The overall wound healing pathway and foreign body response to medical implants warrants further clinical investigation. A more obvious therapeutic benefit for NSAID-peptides is provided via inhibition of nociception and pain receptors linked to COX.[66] Reduction in pain can be linked to improvement in wound healing and patient prognosis.[67]

Hemolysis and cell viability

To evaluate cell biocompatibility of NSAID-peptides, they were incubated with an International Standard (ISO) cell line utilized for biomaterial testing (NCTC 929 murine fibroblast subcutaneous connective tissue). Fibroblasts are appropriate as they are one of the major cell types involved both in wound healing and adherence to implanted medical devices.[11] Four separate assays were performed using alamarBlue® cell viability, hemolysis,

LDH quantification and LIVE/DEAD® staining. The results suggest that NSAID-peptide nanomaterials are biocompatible and may be suitable for use within a range of biomaterial and topical applications. No significant reduction was observed in cell viability after 24 hour exposure to varying concentrations of NSAID-peptides (20-500 μM) utilizing an alamarBlue® cell viability assay (Fig. 7). Cationic NSAID-peptides demonstrate reduced toxicity against mammalian cells due to inherent differences in the membrane potential gradient and lipid composition of bacterial and mammalian cell membranes. Eukaryotic cells are composed of zwitterionic lipids (sterols, cholesterol, phosphatidylcholine, sphingomyelin) whereas bacterial cells are derived from anionic phospholipids.[68] Positively charged NSAID-peptide therefore interact preferentially with negatively charged bacterial cell membranes as confirmed by a hemolysis assay (Fig. S16), commonly utilized to determine the membrane selectivity of antimicrobial peptides.[18,32,69] No significant hemolysis was observed upon NSAID-peptide (20-500 μM) exposure to equine erythrocytes relative to a PBS negative control. Cell cytocompatibility was confirmed via quantification of the toxicity marker LDH (Figure S17). In all instances the mean level of LDH was less than the negative control (PBS) resulting in negative percentage toxicity values. A LIVE/DEAD® Viability/Cytotoxicity assay provided qualitative evidence of NSAID-peptide via fluorescent microscopy imaging (Figures S18-S20). The majority of cells stained green with calcein after 24 hours exposure across all concentrations (20-500 μM) as confirmed by quantitative counting of viable and non-viable cells (Figure S21). The results for each cytotoxicity assay correlate strongly with each other. For example LIVE/DEAD® counting for 500 μM NpxFFKK resulted in 97% viability which is in good agreement with 95% viability obtained at the same concentration for the alamarBlue® cell viability assay.

Conclusions

In summary, we have created a new class of NSAID-peptides with the ability to form defined nanostructures with multiple biofunctional properties (antimicrobial, anti-inflammatory, hydrogel forming). NpxFFKK displays particular promising forming a viscoelastic biocompatible hydrogel with improved COX-2 selectivity and the ability to target antimicrobial resistant bacteria implicated in the most severe nosocomial infections. These hydrogel formulations may be beneficial in the treatment of chronic infected wounds, where a heightened inflammatory response to infection leads to impaired healing. The next stage in development would be to demonstrate their beneficial effects in an *in vivo*, clinical wound environment closely monitoring the effect of NSAID-peptides on inflammatory mediators. Their ultrashort, low molecular weight structure makes their synthesis more amenable to cost-effective upscale by the pharmaceutical industry compared to larger peptides and proteins. This work provides an example of multifunctional peptide hydrogelators that will contribute to the development of future biofunctional nanomaterial therapies, especially within biomaterial applications (wound dressings, medical implants, prostheses), thereby increasing the available treatment options to clinicians and patients and limiting the increasing threat of antimicrobial resistance.

Acknowledgements

This work was supported by the Queen's University Research Support Package for New Academic Staff for and a Royal Society Research Grant (RG150171) for GL. APM acknowledges funding provided by a N. Ireland Department of Employment and Learning PhD studentship grant. The manuscript was written through contributions of all authors. All authors have given approval to the final version of the manuscript. APM, SG, ERD, JZ, SP, BFG and BX contributed equally. We acknowledge help from Prof. Dave Adams (University

of Liverpool) for allowing us access to his Anton Paar Physica MCR301 rheometer for rheological studies.

References

1 J. O'Neill, *The Review on Antimicrobial Resistance: UK Government Report*, London, 2015.

2 Centre for Disease control (CDC), *Data from the National Hospital Discharge Survey. Available: http://www.cdc.gov/nchs/data/nhds/4procedures/2010pro_numberpercentage.pdf*, 2010.

3 P. Astagneau, C. Rioux, F. Golliot, G. Brucker and INCISO Network Study Group, *J. Hosp. Infect.*, 2001, **48**, 267-274.

4 S. Guo and L. A. Dipietro, *J. Dent. Res.*, 2010, **89**, 219-229.

5 F. Gottrup, *Am. J. Surg.*, 2004, **187**, 38S-43S.

6 N. B. Menke, K. R. Ward, T. M. Witten, D. G. Bonchev and R. F. Diegelmann, *Clin. Dermatol.*, 2007, **25**, 19-25.

7 P. C. Konturek, T. Brzozowski, S. J. Konturek, S. Kwiecien, A. Dembinski and E. G. Hahn, *Scand. J. Gastroenterol.*, 2001, **36**, 1239-1247.

8 M. Ståhle, in *Antimicrobial Peptides and Innate Immunity*, ed. P. S. Hiemstra and S. A. J. Zaat, Springer, Basel, 2013, p. 123-129.

9 G. D. Krischak, P. Augat, L. Claes, L. Kinzl and A. Beck, *J. Wound Care*, 2007, **16**, 76-78.

10 S. M. Hamilton, C. R. Bayer, D. L. Stevens and A. E. Bryant, *J. Infect. Dis.*, 2014, **209**, 1429-1435.

11 J. M. Morais, F. Papadimitrakopoulos and D. J. Burgess, *AAPS J.*, 2010, **12**, 188-196.

12 P. Price, K. Fogh, C. Glynn, D. L. Krasner, J. Osterbrink and R. G. Sibbald, *Int. Wound. J.*, 2007, **4 Suppl 1**, 1-3.

13 G. Laverty, S. P. Gorman and B. F. Gilmore, *Int. J. Mol. Sci.*, 2011, **12**, 6566-6596.

14 G. Laverty, S. P. Gorman and B. F. Gilmore, *J. Biomed. Mater. Res. A.*, 2012, **100**, 1803-1814.

15 R. T. Cleophas, J. Sjollema, H. J. Busscher, J. A. Kruijtzer and R. M. Liskamp, *Biomacromolecules*, 2014, **15**, 3390-3395.

16 Z. Xie, N. V. Aphale, T. D. Kadapure, A. S. Wadajkar, S. Orr, D. Gyawali, G. Qian, K. T. Nguyen and J. Yang, *J. Biomed. Mater. Res. A.*, 2015, **103**, 3907-3918.

17 V. W. Ng, J. M. Chan, H. Sardon, R. J. Ono, J. M. Garcia, Y. Y. Yang and J. L. Hedrick, *Adv. Drug Deliv. Rev.*, 2014, **78**, 46-62.

18 G. Laverty, A. P. McCloskey, B. F. Gilmore, D. S. Jones, J. Zhou and B. Xu, *Biomacromolecules*, 2014, .

19 M. J. Webber, J. B. Matson, V. K. Tamboli and S. I. Stupp, *Biomaterials*, 2012, **33**, 6823-6832.

20 F. Zhao, M. L. Ma and B. Xu, *Chem. Soc. Rev.*, 2009, **38**, 883-891.

21 J. Majumder, M. R. Das, J. Deb, S. S. Jana and P. Dastidar, *Langmuir*, 2013, **29**, 10254-10263.

22 D. M. Ryan, S. B. Anderson, F. T. Senguen, R. E. Youngman and B. L. Nilsson, *Soft Matter*, 2010, **6**, 475-479.

23 E. R. Draper, K. L. Morris, M. A. Little, J. Raeburn, C. Colquhoun, E. R. Cross, T. O. McDonald, L. C. Serpell and D. J. Adams, *Cryst. Eng. Comm.*, 2015, **17**, 8047-8057.

24 Z. Yang, G. Liang, M. Ma, Y. Gao and B. Xu, *J. Mater. Chem*, 2007, **17**, 850-854.

25 J. Y. Li, Y. Kuang, J. F. Shi, Y. Gao, J. Zhou and B. Xu, *Beilstein J. Org. Chem.*, 2013, **9**, 908-917.

26 J. Y. Li, X. Li, Y. Kuang, Y. Gao, X. Du, J. Shi and B. Xu, *Adv. Healthc. Mater.,* 2013, **2**, 1586-1590.

27 A. Y. Mensah, P. J. Houghton, R. A. Dickson, T. C. Fleischer, M. Heinrich and P. Bremner, *Phytother. Res.,* 2006, **20**, 941-944.

28 C. Gong, Q. Wu, Y. Wang, D. Zhang, F. Luo, X. Zhao, Y. Wei and Z. Qian, *Biomaterials,* 2013, **34**, 6377-6387.

29 S. Bhuniya, Y. J. Seo and B. H. Kim, *Tetrahedron Lett,* 2006, **47**, 7153-7156.

30 D. J. Adams, M. F. Butler, W. J. Frith, M. Kirkland, L. Mullen and P. Sanderson, *Soft Matter,* 2009, **5**, 1856-1862.

31 A. G. Pogorelov and I. I. Selezneva, *Bull. Exp. Biol. Med.,* 2010, **150**, 153-156.

32 L. Jiang, D. Xu, T. J. Sellati and H. Dong, *Nanoscale,* 2015, **7**, 19160-19169.

33 M. Mateescu, S. Baixe, T. Garnier, L. Jierry, V. Ball, Y. Haikel, M. H. Metz-Boutigue, M. Nardin, P. Schaaf, O. Etienne and P. Lavalle, *PLoS One,* 2015, **10**, e0145143.

34 G. Laverty, M. McLaughlin, C. Shaw, S. P. Gorman and B. F. Gilmore, *Chem. Biol. Drug Des.,* 2010, **75**, 563-569.

35 L. Chen, S. Revel, K. Morris, L. C Serpell and D. J. Adams, *Langmuir,* 2010, **26**, 13466-13471.

36 A. P. McCloskey, B. F. Gilmore and G. Laverty, *Pathogens,* 2014, **3**, 791-821.

37 P. Cioni and G. B. Strambini, *Biophys. J.,* 2002, **82**, 3246-3253.

38 A. K. Soper and C. J. Benmore, *Phys. Rev. Lett.,* 2008, **101**, 065502.

39 M. Conda-Sheridan, S. S. Lee, A. T. Preslar and S. I. Stupp, *Chem. Commun. (Camb),* 2014, **50**, 13757-13760.

40 M. L. Muro-Small, J. Chen and A. J. McNeil, *Langmuir,* 2011, **27**, 13248-13253.

41 M. Kolbel and F. M. Menger, *Chem. Commun.,* 2001, , 275-276.

42 L. A. Estroff and A. D. Hamilton, *Chem. Rev.,* 2004, **104**, 1201-1218.

43 V. Jayawarna, S. M. Richardson, A. R. Hirst, N. W. Hodson, A. Saiani, J. E. Gough and R. V. Ulijn, *Acta Biomater.*, 2009, **5**, 934-943.

44 C. Tang, A. M. Smith, R. F. Collins, R. V. Ulijn and A. Saiani, *Langmuir*, 2009, **25**, 9447-9453.

45 G. A. Pankey and L. D. Sabath, *Clin. Infect. Dis.*, 2004, **38**, 864-870.

46 J. Li, Y. Kuang, Y. Gao, X. Du, J. Shi and B. Xu, *J. Am. Chem. Soc.*, 2013, **135**, 542-545.

47 D. Xu, L. Jiang, A. Singh, D. Dustin, M. Yang, L. Liu, R. Lund, T. J. Sellati and H. Dong, *Chem. Commun. (Camb)*, 2015, **51**, 1289-1292.

48 P. Li, Y. F. Poon, W. Li, H. Y. Zhu, S. H. Yeap, Y. Cao, X. Qi, C. Zhou, M. Lamrani, R. W. Beuerman, E. T. Kang, Y. Mu, C. M. Li, M. W. Chang, S. S. Leong and M. B. Chan-Park, *Nat. Mater.*, 2011, **10**, 149-156.

49 D. A. Salick, J. K. Kretsinger, D. J. Pochan and J. P. Schneider, *J. Am. Chem. Soc.*, 2007, **129**, 14793-14799.

50 D. A. Salick, D. J. Pochan and J. P. Schneider, *Adv. Mater.*, 2009, **21**, 4120-4123.

51 A. S. Veiga, C. Sinthuvanich, D. Gaspar, H. G. Franquelim, M. A. Castanho and J. P. Schneider, *Biomaterials*, 2012, **33**, 8907-8916.

52 E. A. Grice and J. A. Segre, *Adv. Exp. Med. Biol.*, 2012, **946**, 55-68.

53 R. D. Wolcott, D. D. Rhoads, M. E. Bennett, B. M. Wolcott, L. Gogokhia, J. W. Costerton and S. E. Dowd, *J. Wound Care*, 2010, **19**, 45-6, 48-50, 52-3.

54 R. D. Wolcott and D. D. Rhoads, *J. Wound Care*, 2008, **17**, 145-8, 150-2, 154-5.

55 Z. Yin, Y. Wang, L. R. Whittell, S. Jergic, M. Liu, E. Harry, N. E. Dixon, M. J. Kelso, J. L. Beck and A. J. Oakley, *Chem. Biol.*, 2014, **21**, 481-487.

56 S. C. Mansour, C. de la Fuente-Nunez and R. E. Hancock, *J. Pept. Sci.*, 2015, **21**, 323-329.

57 E. F. Haney, S. C. Mansour, A. L. Hilchie, C. de la Fuente-Nunez and R. E. Hancock, *Peptides*, 2015, **71**, 276-285.

58 K. C. Duggan, M. J. Walters, J. Musee, J. M. Harp, J. R. Kiefer, J. A. Oates and L. J. Marnett, *J. Biol. Chem.*, 2010, **285**, 34950-34959.

59 F. E. Silverstein, G. Faich, J. L. Goldstein, L. S. Simon, T. Pincus, A. Whelton, R. Makuch, G. Eisen, N. M. Agrawal, W. F. Stenson, A. M. Burr, W. W. Zhao, J. D. Kent, J. B. Lefkowith, K. M. Verburg and G. S. Geis, *JAMA*, 2000, **284**, 1247-1255.

60 P. K. Vemula, J. Li and G. John, *J. Am. Chem. Soc.*, 2006, **128**, 8932-8938.

61 A. Futagami, M. Ishizaki, Y. Fukuda, S. Kawana and N. Yamanaka, *Lab. Invest.*, 2002, **82**, 1503-1513.

62 E. A. Blomme, K. S. Chinn, M. M. Hardy, J. J. Casler, S. H. Kim, A. C. Opsahl, W. A. Hall, D. Trajkovic, K. N. Khan and C. S. Tripp, *Br. J. Dermatol.*, 2003, **148**, 211-223.

63 T. A. Wilgus, Y. Vodovotz, E. Vittadini, E. A. Clubbs and T. M. Oberyszyn, *Wound Repair Regen.*, 2003, **11**, 25-34.

64 T. A. Wilgus, V. K. Bergdall, K. L. Tober, K. J. Hill, S. Mitra, N. A. Flavahan and T. M. Oberyszyn, *Am. J. Pathol.*, 2004, **165**, 753-761.

65 M. Kastellorizios, N. Tipnis and D. J. Burgess, in *Immune Responses to Biosurfaces*, ed. J. D. Lambris, K. N. Ekdahl, D. Ricklin and D. Nilsson, Springer International Publishing, Switzerland, 2015, p. 93-108.

66 S. Bingham, P. J. Beswick, D. E. Blum, N. M. Gray and I. P. Chessell, *Semin. Cell Dev. Biol.*, 2006, **17**, 544-554.

67 L. McGuire, K. Heffner, R. Glaser, B. Needleman, W. Malarkey, S. Dickinson, S. Lemeshow, C. Cook, P. Muscarella, W. S. Melvin, E. C. Ellison and J. K. Kiecolt-Glaser, *Ann. Behav. Med.*, 2006, **31**, 165-172.

68 A. J. Mason, A. Marquette and B. Bechinger, *Biophys. J.*, 2007, **93**, 4289-4299.

69 G. Laverty, A. P. McCloskey, S. P. Gorman and B. F. Gilmore, *J. Pept. Sci.*, 2015, **21**, 770-778.

Figures

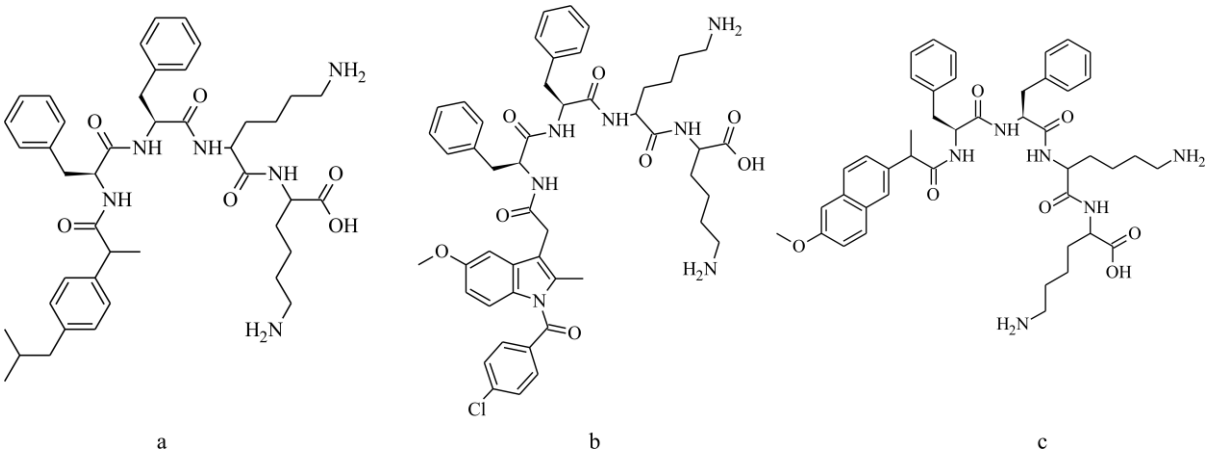

Fig. 1 Chemical structures of NSAID-peptides investigated: (a) IbuFFKK, (b) IndFFKK, (c) NpxFFKK.

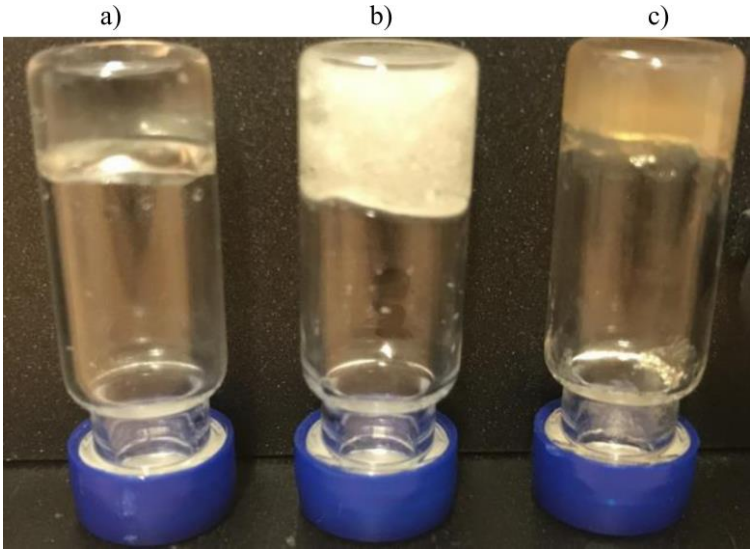

Fig. 2 Gel inversion assay for 2% w/v pH 7.4 (a) IbuFFKK, D_2O primary vehicle, (b) IndFFKK, H_2O primary vehicle (c) NpxFFKK, H_2O primary vehicle.

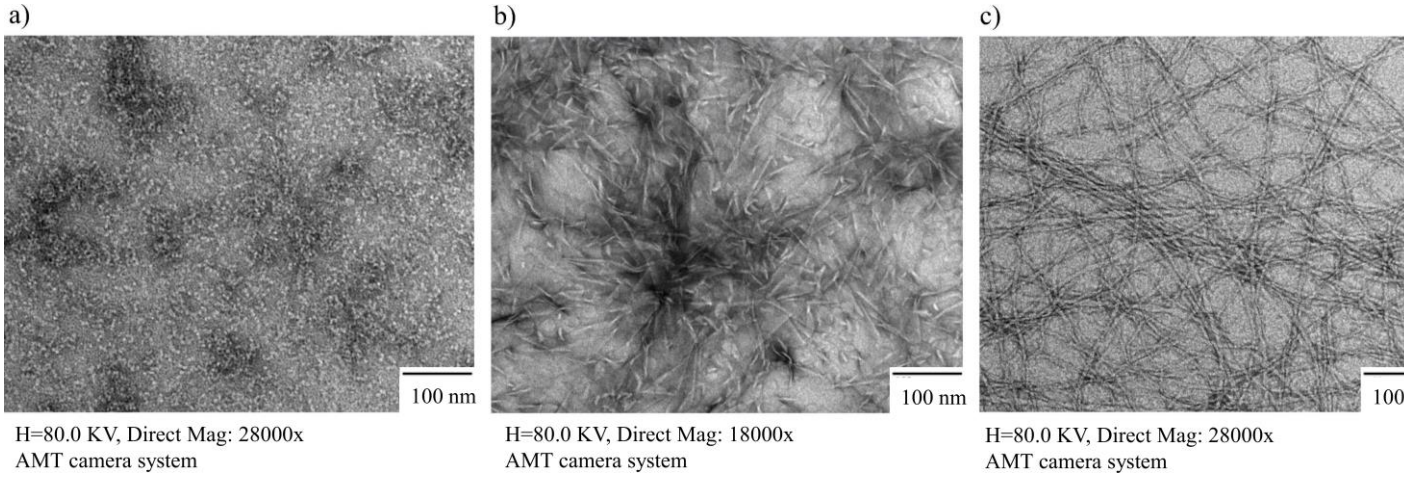

Fig. 3 Transmission electron microscopy (TEM) images of 2% w/v (a) IbuFFKK (28,000x, D_2O), (b) IndFFKK (18,000x, H_2O), (c) NpxFFKK (28,000x, H_2O).

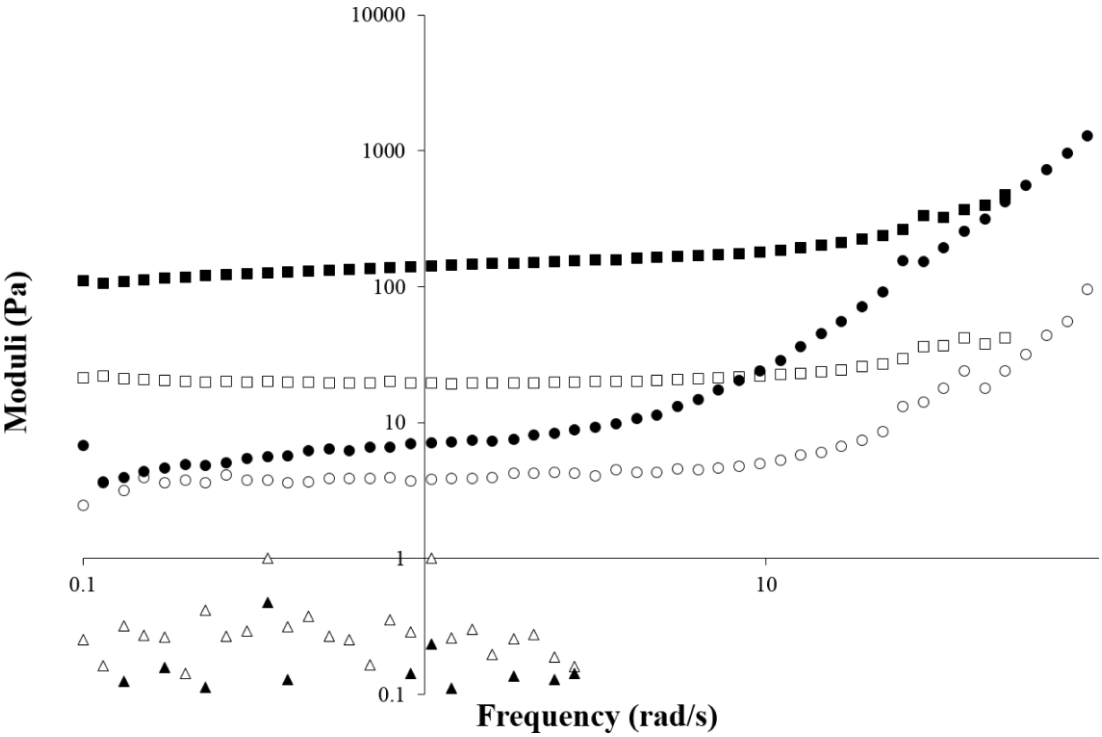

Fig. 4 Oscillatory frequency sweep 2% w/v NSAID-peptides. Key: black triangle: G′ IbuFFKK, white triangle: G″ IbuFFKK black circle: G′ IndFFKK, white circle: G″ IndFFKK, black square: G′ NpxFFKK, white square: G″ NpxFFKK.

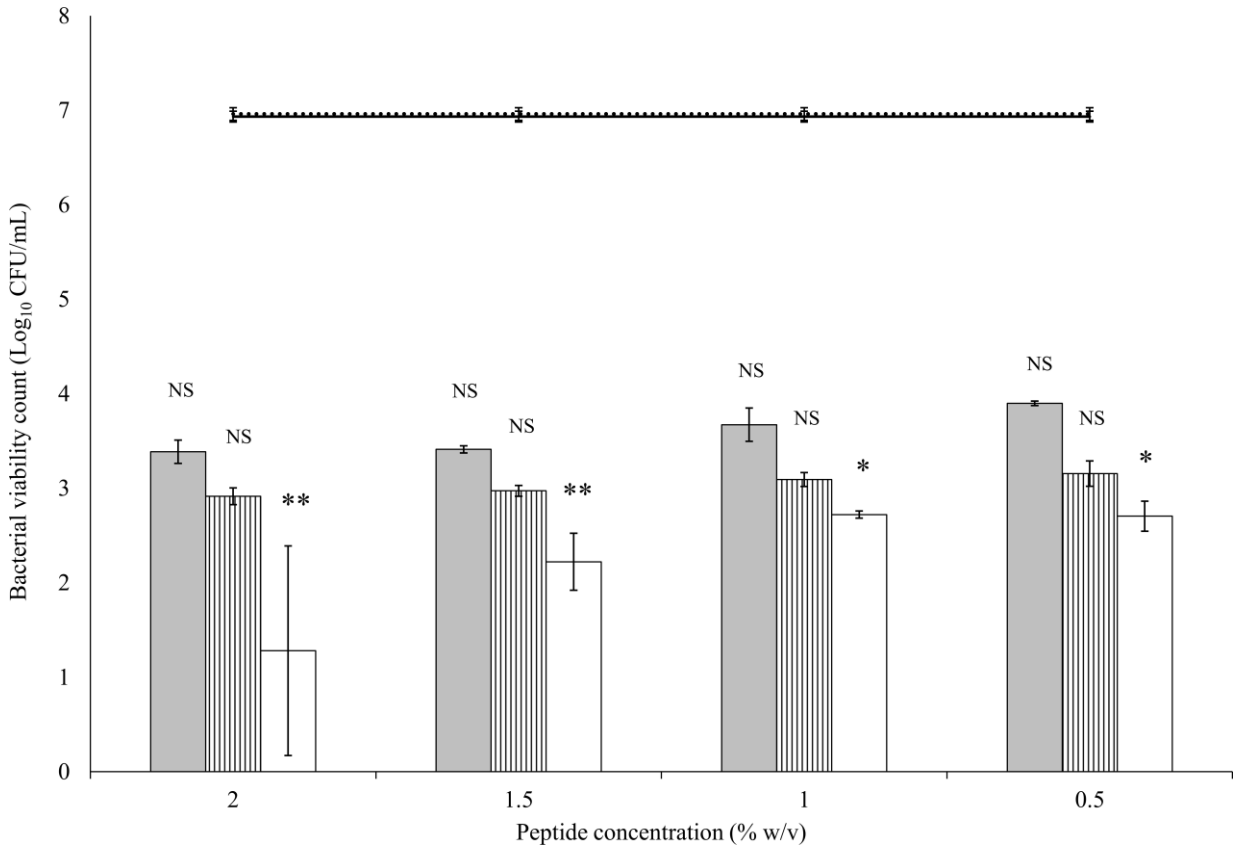

Fig. 5 Logarithmic reduction in *S. aureus* (ATCC 6584) viable count (Log_{10} CFU/mL) after 24 hour incubation with varying concentrations of NSAID-peptides. Results are displayed as a mean of six replicates. Key: grey column: IbuFFKK, striped column: IndFFKK, white column: NpxFFKK, dotted line: PBS control, black line: 2% w/v HPMC control. NS: no significant difference ($P \geq 0.05$), *: $P < 0.05$, **: $P < 0.01$ significant difference between Log_{10} CFU/mL of NSAID-peptide and the negative control (PBS).

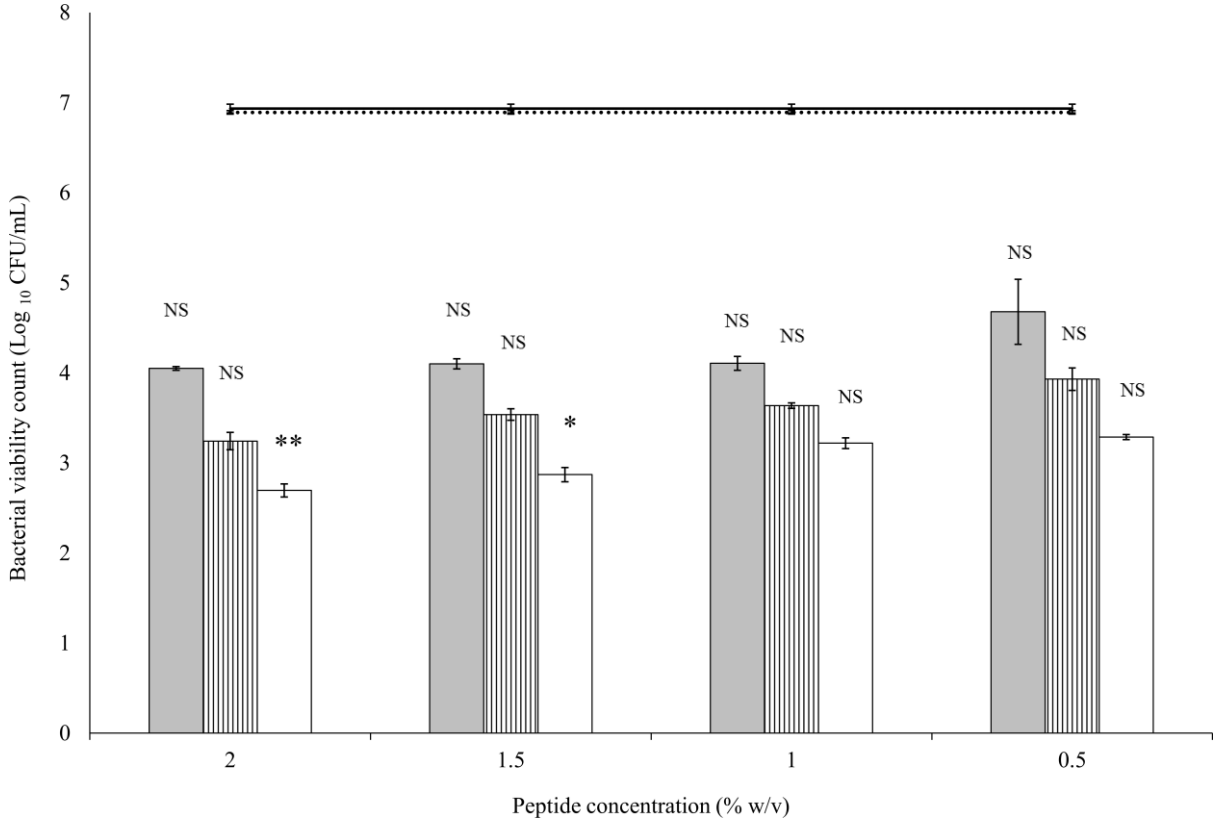

Fig. 6 Logarithmic reduction in *P. aeruginosa* (PAO1) viable count (Log_{10} CFU/mL) after 24 hour incubation with varying concentrations of NSAID-peptides. Results are displayed as a mean of six replicates. Key: grey column: IbuFFKK, striped column: IndFFKK, white column: NpxFFKK, dotted line: PBS control, black line: 2% w/v HPMC control. NS: no significant difference ($P \geq 0.05$), *: $P < 0.05$, **: $P < 0.01$ significant difference between Log_{10} CFU/mL of NSAID-peptide and the negative control (PBS).

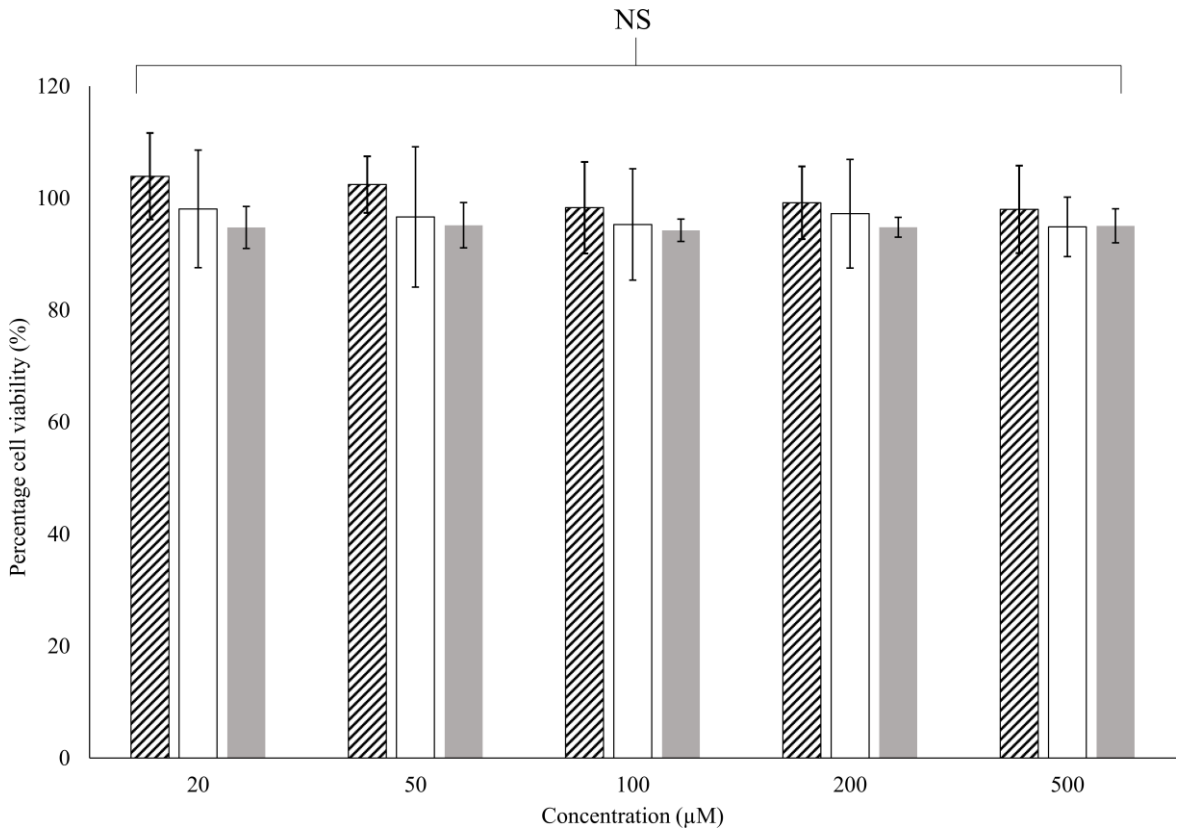

Fig. 7 Percentage cell viability of NCTC clone 929 (ATCC CCL 1) cells after 24 hour exposure to varying concentrations of NSAID-peptides. Key: striped: IbuFFKK, white: IndFFKK, grey: NpxFFKK, ns: no significant difference (P≥0.05) between the NSAID-peptide and the negative control (PBS).

Supporting Information

Self-assembling Ultrashort NSAID-Peptide Nanosponges: Multifunctional Antimicrobial and Anti-inflammatory Materials

*Alice P. McCloskey, Sophie M. Gilmore, Jie Zhou, Emily R. Draper, Simon Porter, Brendan F. Gilmore, Bing Xu, Garry Laverty**

Ibuprofen-L-phenylalanine-L-phenylalanine-L-Lysine-L-Lysine-COOH (IbuFFKK). ^{1}H NMR (400 MHz, DMSO-d_6, δ): 8.21-8.02 (m, *J* = 4.06, 4H; NH), 7.66 (s, *J* = 4.13, 4H; NH_2), 7.25-6.99 (m, *J* = 14.26, 14H; Ar H), 4.57-4.18 (m, *J* = 4.40, 4H, C*H*NH), 3.03 (q, *J* = 1.08, 1H;

C*H*CH$_3$), 2.84-2.68 (m, *J* = 10.75, 8H; CH$_2$Ar, 2H; C*H*$_2$NH$_2$), 2.39 (d, *J* = 3.23, 3H; CH$_3$), 1.54-1.07 (m, *J* = 17.54, 2H; Ar C*H*$_2$CH(CH$_3$)$_2$, 1H; CH$_2$C*H*(CH$_3$)$_2$, 12H; CH$_2$), 0.86-0.83 (m, *J* = 6.51, 6H; CH$_3$). EIMS *m*/*z* (%): 756.46 (100) [M$^+$], 757.46 (46.5) [M$^+$ +H]$^+$, 758.46 (10.6) [M$^+$+2H]$^+$; (ESI) *m*/*z*: [M + H]$^+$ calcd for $C_{43}H_{60}N_6O_6$, 756.99; found, 756.46.

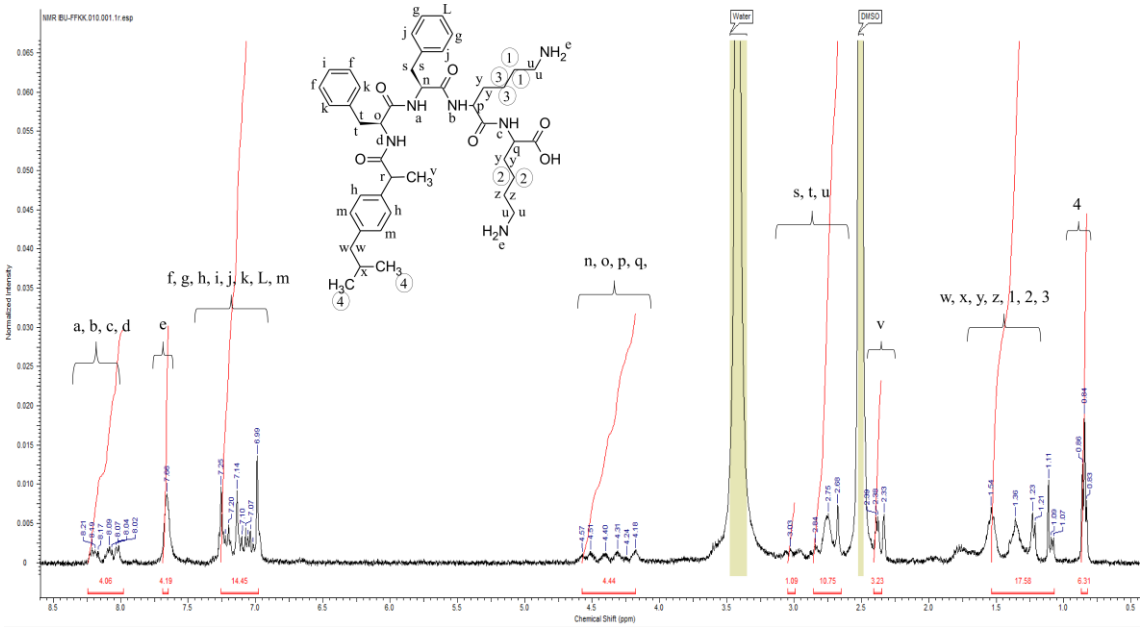

Figure S1. ^{1}H NMR.spectra for IbuFFKK (C_2D_6OS, TMS standard, 400MHZ).

Indomethacin-L-phenylalanine-L-phenylalanine-L-Lysine-L-Lysine-COOH (IndFFKK). ^{1}H NMR (400 MHz, DMSO-d_6, δ): 8.21-8.16 (m, *J* = 2.59, 1H; NH, 1H; Ar H), 7.63-7.55 (m, *J* = 4.16, 1H; Ar H, 2H; NH), 7.22-6.62 (m, *J* = 17.33, 14H; Ar H, 1H; NH, 4H; NH$_2$), 4.56-4.16 (m, *J* = 5.49, 4H; C*H*NH), 3.74-3.67 (m, *J* = 4.41, 3H; CH$_3$, 2H; CH$_2$CO), 3.03-2.68 (m, *J* = 14.50, 4H; C*H*$_2$NH$_2$, 4H; C*H*$_2$ Ar), 2.33 (s, *J* = 3.02, 3H; CH$_3$), 1.89-1.24 (m, *J* = 21.08, 12H; CH$_2$). EIMS *m*/*z* (%): 893.39 (100) [M$^+$], 894.39 (51.9) [M$^+$ − H], 895.38 (32) [M$^+$ − 2H], 896.39 (16.6); (ESI) *m*/*z*: [M + H]$^+$ calcd for $C_{49}H_{58}ClN_7O_8$, 894.47; found, 893.39.

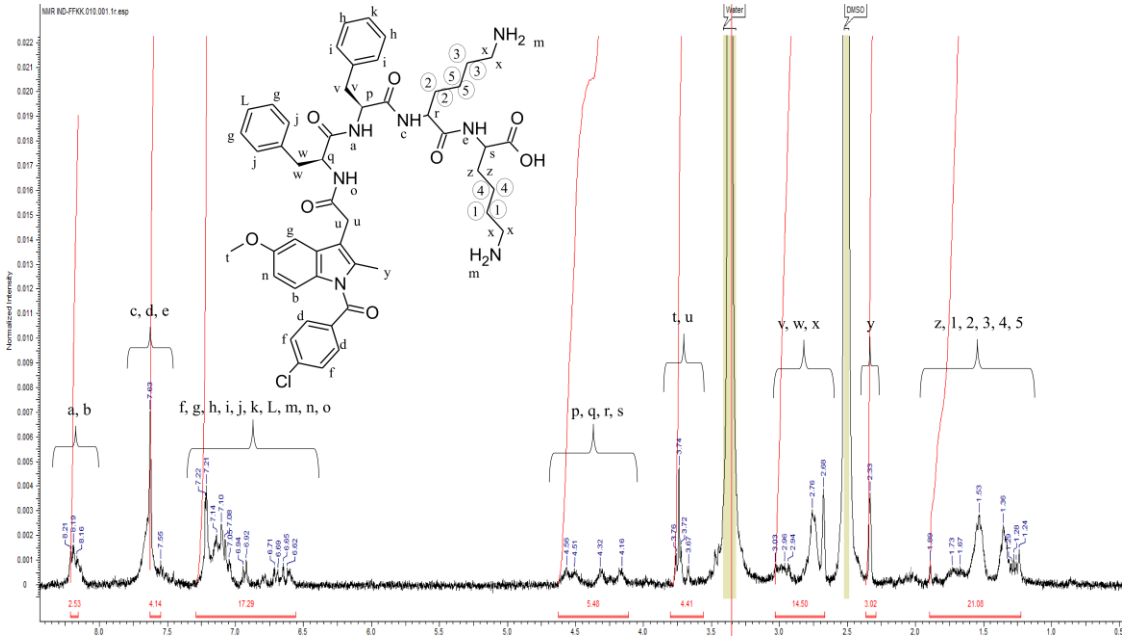

Figure S2. ^{1}H NMR.spectra for IndFFKK (C_2D_6OS, TMS standard, 400MHZ).

Naproxen-L-phenylalanine-L-phenylalanine-L-Lysine-L-Lysine-COOH (NpxFFKK).

^{1}H NMR (400 MHz, DMSO-d_6, δ): 8.22-8.04 (m, *J* = 5.53, 3H; NH, 2H; Ar H), 7.75-7.05 (m, *J* = 21.43, 14H; Ar H, 4H; NH_2), 4.50-3.71 (m, *J* = 6.20**,** 4H; C*H*NH, 1H; Ar C*H*CH_3), 2.98-2.68 (m, *J* = 9.97 4H; Ar CH_2, 4H; C*H*$_2$$NH_2$), 2.33 (s, *J* = 3.10, 3H; CH_3), 1.73-1.03 (m, *J* = 21.71**,** 12H; CH_2, 3H; CH_3). EIMS *m*/*z* (%): 780.42 (100) [M^+], 781.42 (47.6) [$M^+ - H$], 782.43 (11.1) [$M^+ - 2H$]; (ESI) *m*/*z*: [M + H]$^+$ calcd for $C_{44}H_{56}N_6O_7$, 780.97; found, 780.42.

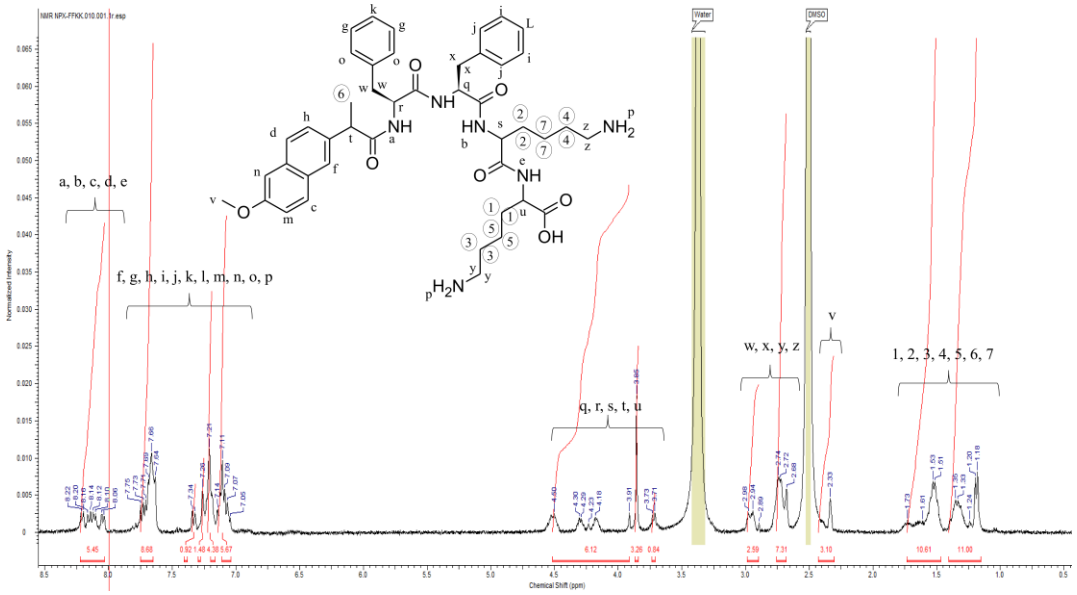

Figure S3. ^{1}H NMR.spectra for NpxFFKK (C_2D_6OS, TMS standard, 400MHZ).

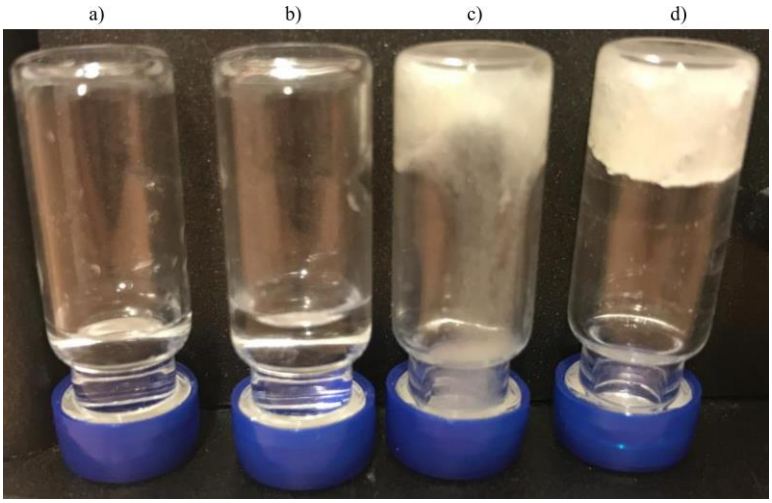

Figure S4. Gel inversion assay for IbuFFKK pH 7.4, H_2O primary vehicle. a) 0.5% w/v, b) 1.0% w/v, c) 1.5% w/v, d) 2.0% w/v.

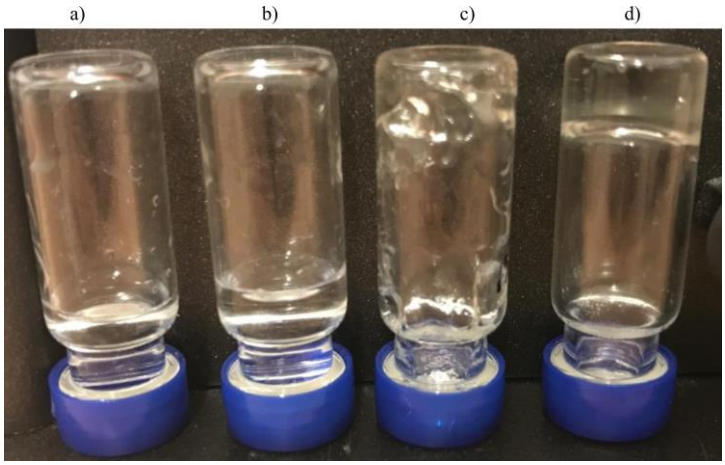

Figure S5. Gel inversion assay for IbuFFKK pH 7.4, D_2O primary vehicle, a) 0.5% w/v, b) 1.0% w/v, c) 1.5% w/v, d) 2.0% w/v.

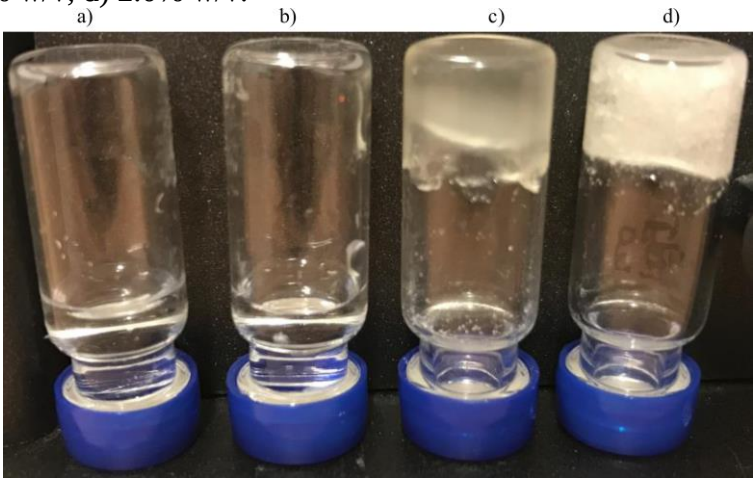

Figure S6. Gel inversion assay for IndFFKK pH 7.4, H_2O primary vehicle, a) 0.5% w/v, b) 1.0% w/v, c) 1.5% w/v, d) 2.0% w/v.

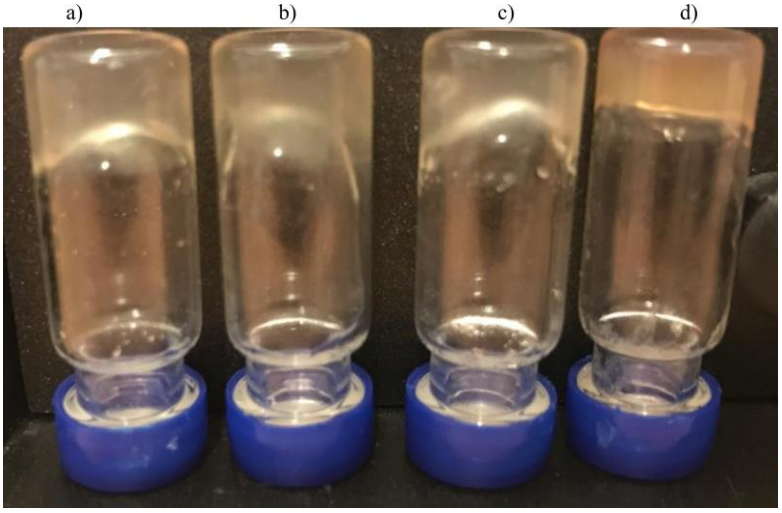

Figure S7. Gel inversion assay for NpxFFKK pH 7.4, H_2O primary vehicle, a) 0.5% w/v, b) 1.0% w/v, c) 1.5% w/v, d) 2.0% w/v

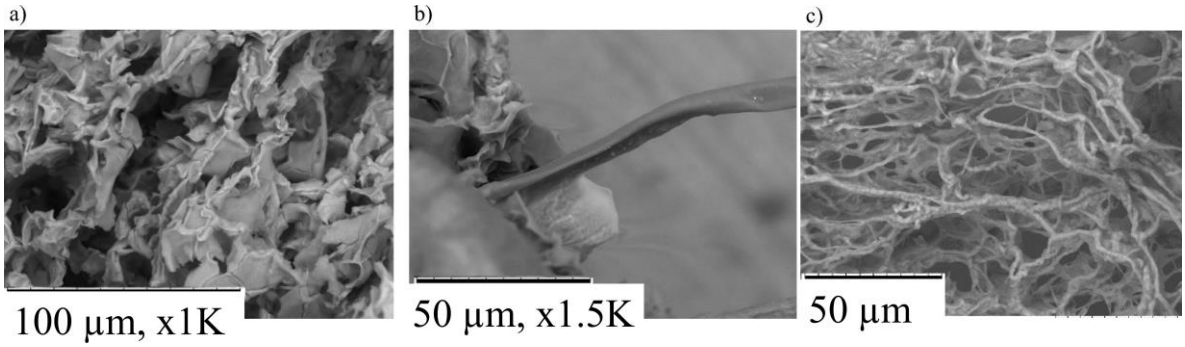

Figure S8. Cryo-SEM images of 2% w/v (a) IbuFFKK (D_2O), (b) IndFFKK (H_2O), (c) NpxFFKK (H_2O).

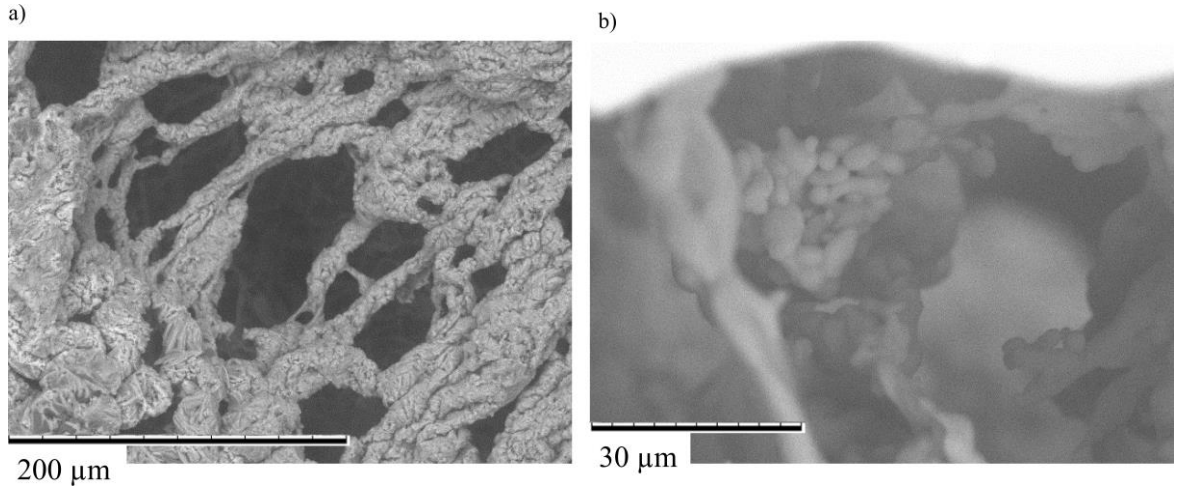

Figure S9. Cryo-SEM images of 2% w/v IbuFFKK (H_2O primary vehicle).

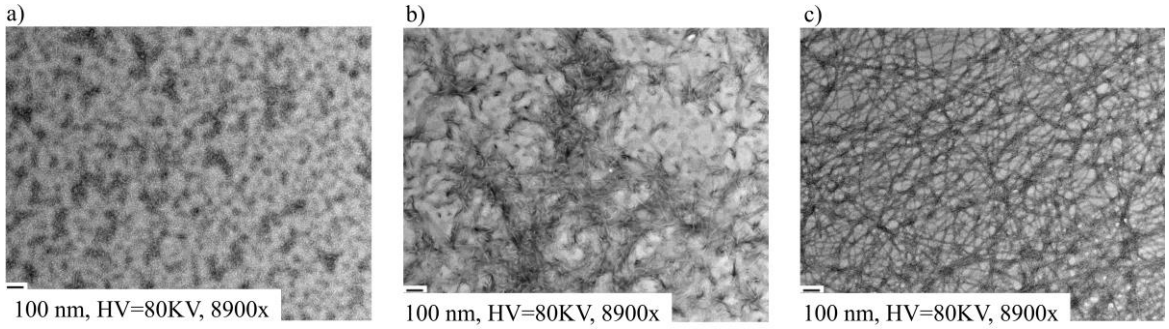

Figure S10. TEM images of 2% w/v (8900x) (a) IbuFFKK (D_2O), (b) IndFFKK (H_2O), (c)NpxFFKK (H_2O).

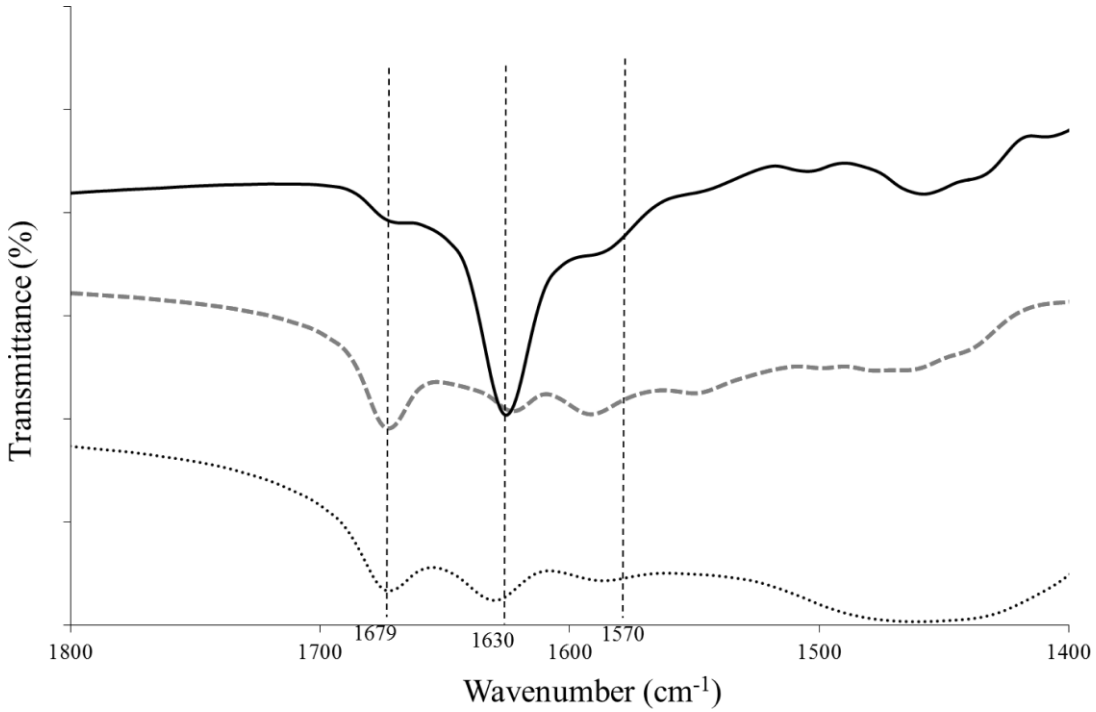

Figure S11. FTIR spectra displaying amide band of 2% w/v NSAID-peptides in deuterated solvents. Key: dotted line: IbuFFKK, dashed line: IndFFKK , full line: NpxFFKK.

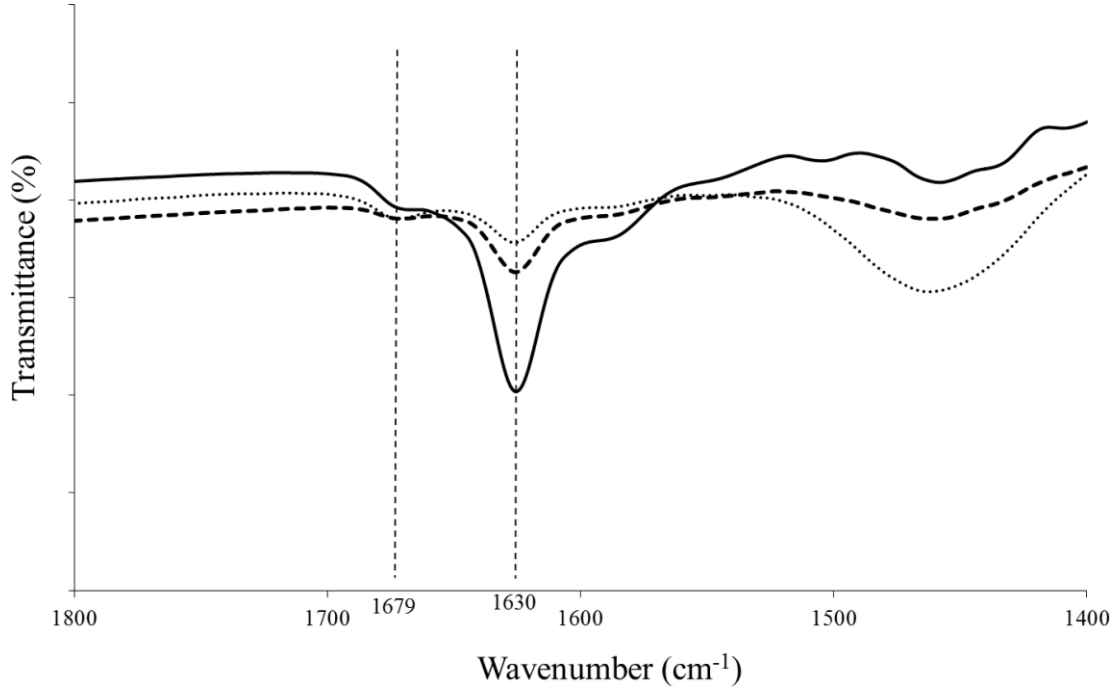

Figure S12. FTIR spectra displaying amide band of 0.5-2% w/v NpxFFKK peptide. Key: dotted line: 0.5% w/v, dashed line: 1.5% w/v, full line: 2% w/v.

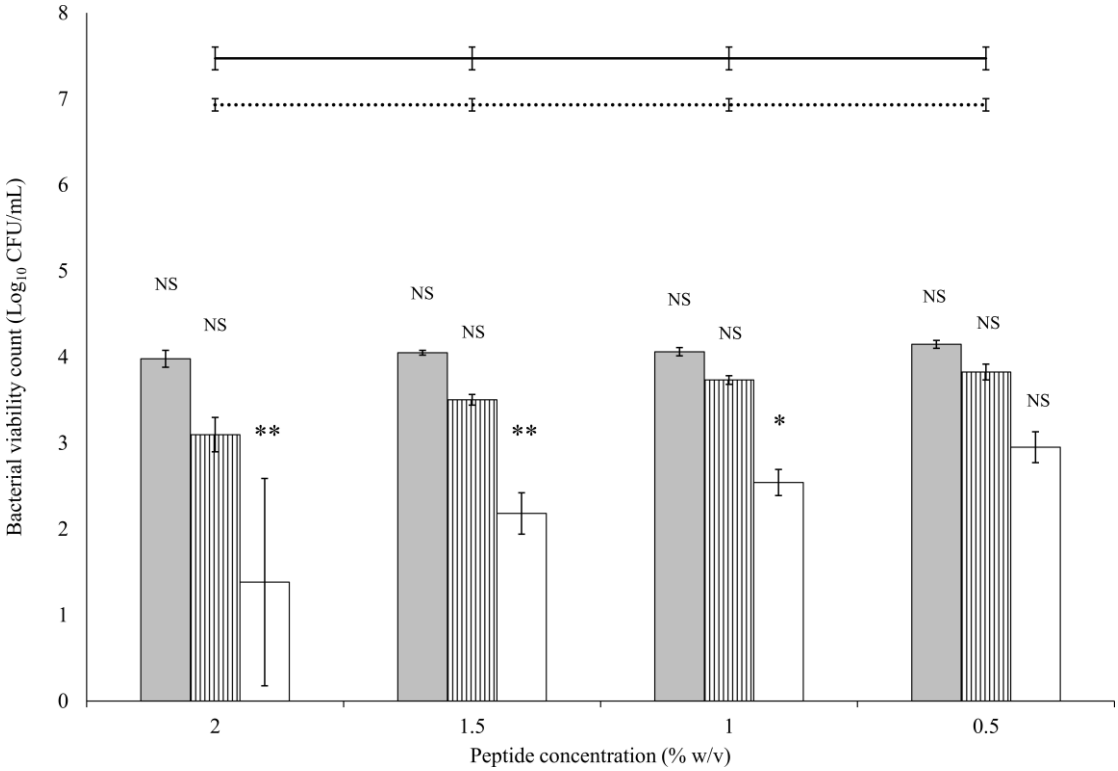

Figure S13. Logarithmic reduction in *S. epidermidis* (ATCC 35984) viable count (Log_{10} CFU/mL) after 24 hour incubation with varying concentrations of NSAID-peptides. Results are displayed as a mean of six replicates. Key: grey column: IbuFFKK, striped column: IndFFKK, white column: NpxFFKK, dotted line: PBS control, black line: 2% w/v HPMC control. NS: no significant difference ($P \geq 0.05$), *: $P < 0.05$, **: $P < 0.01$ significant difference between Log_{10} CFU/mL of NSAID-peptide and the negative control (PBS).

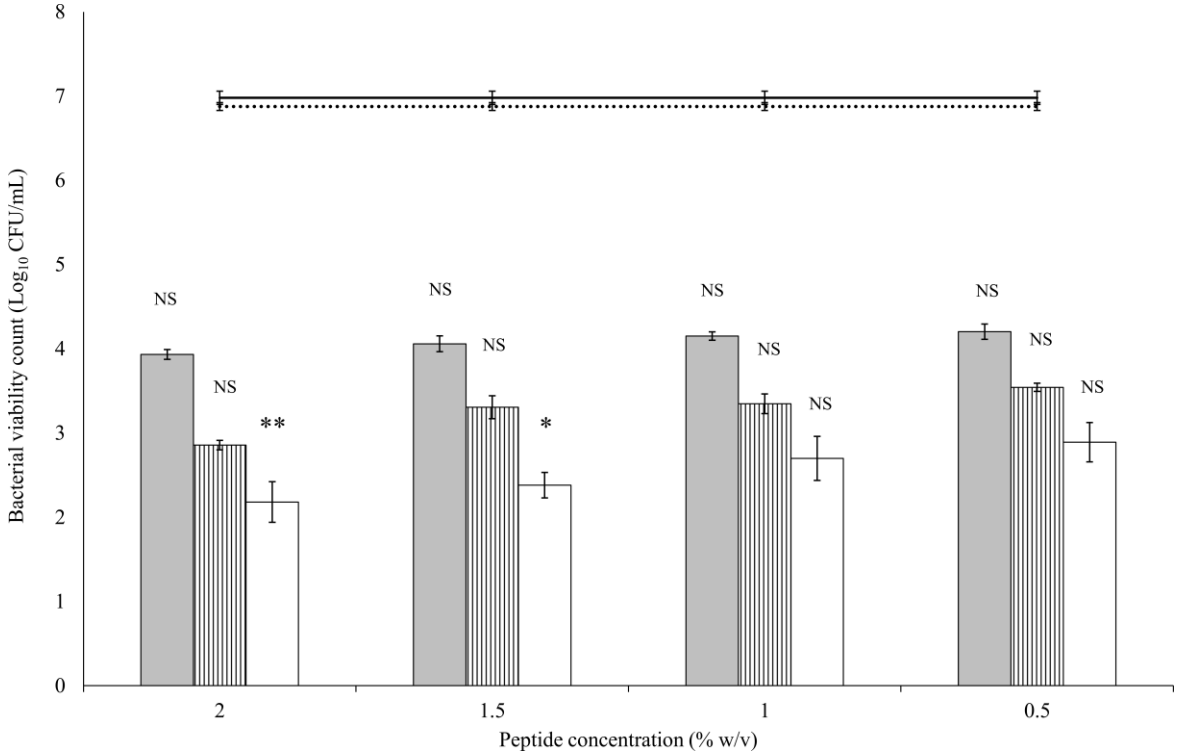

Figure S14. Logarithmic reduction in *E. coli* (ATCC 11303) viable count (Log_{10} CFU/mL) after 24 hour incubation with varying concentrations of NSAID-peptides. Results are displayed as a mean of six replicates. Key: grey column: IbuFFKK, striped column: IndFFKK, white column: NpxFFKK, dotted line: PBS control, black line: 2% w/v HPMC control. NS: no significant difference ($P \geq 0.05$), *: $P < 0.05$, **: $P < 0.01$ significant difference between Log_{10} CFU/mL of NSAID-peptide and the negative control (PBS).

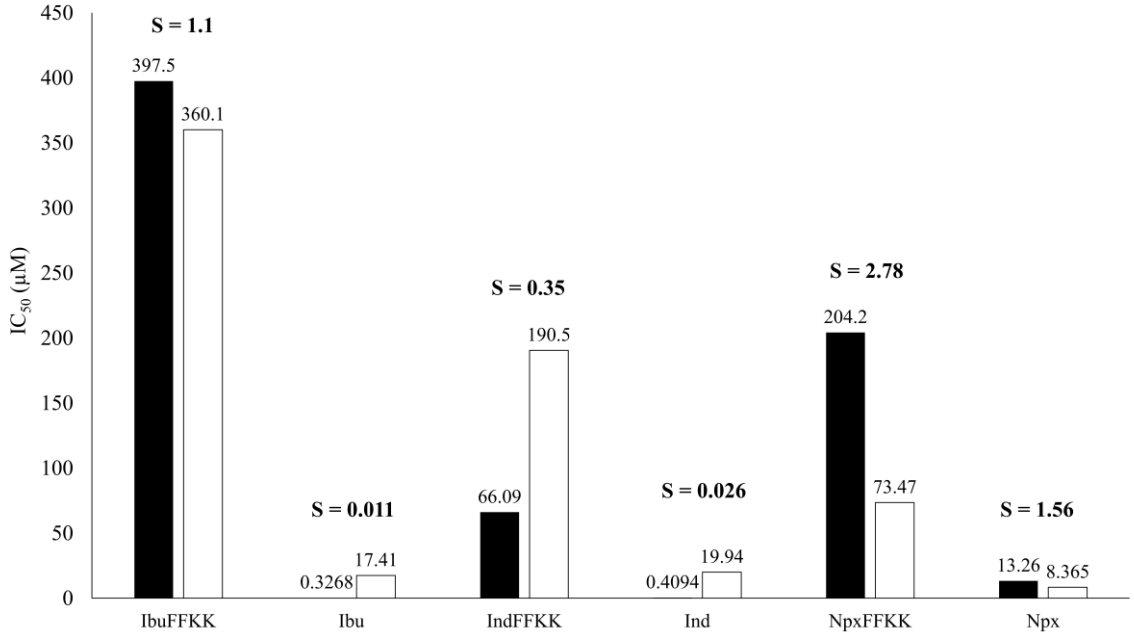

Figure S15. IC_{50} values of NSAID-peptide and NSAIDs only molecules corresponding to inhibition of COX-1 (black column) and COX-2 (white column) enzymes. Selectivity (S) is defined as the ratio of the IC_{50} values relative to COX-1: COX-2.

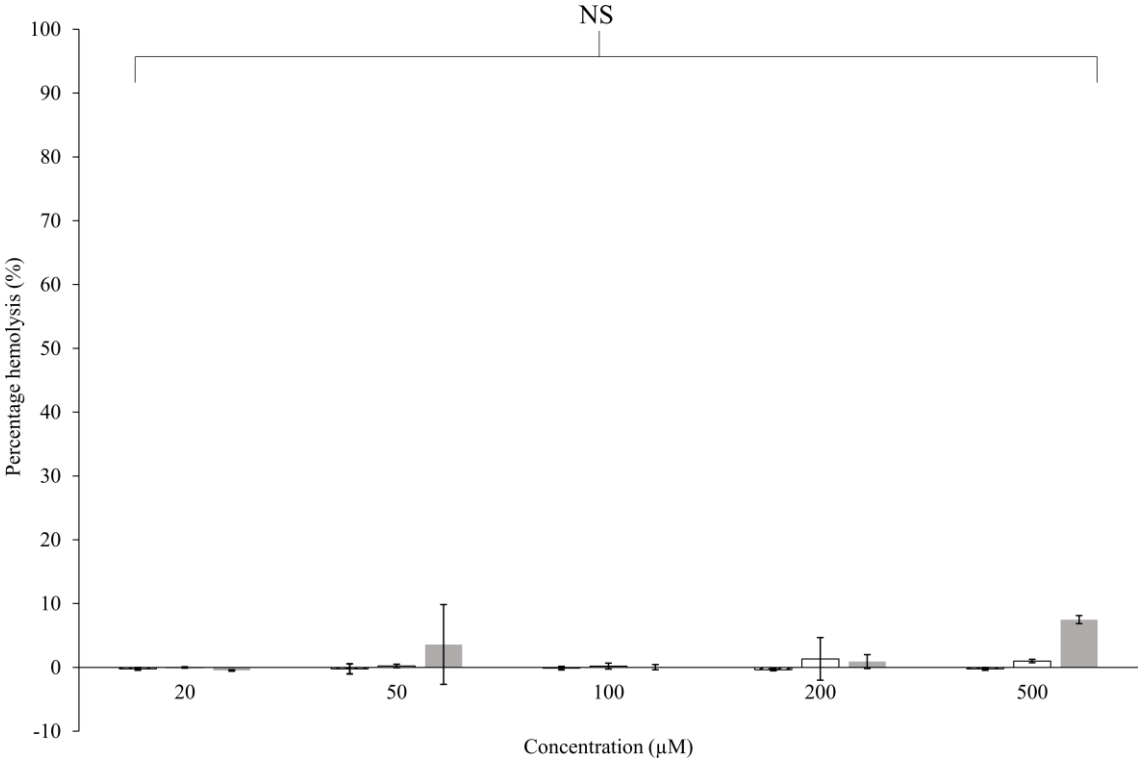

Figure S16. Percentage hemolysis of equine erythrocytes after 1 hour exposure to varying concentrations of NSAID-peptides. Key: striped: IbuFFKK, white: IndFFKK, grey: NpxFFKK, NS: no significant difference (P≥0.05) between the NSAID-peptide and the negative control (PBS).

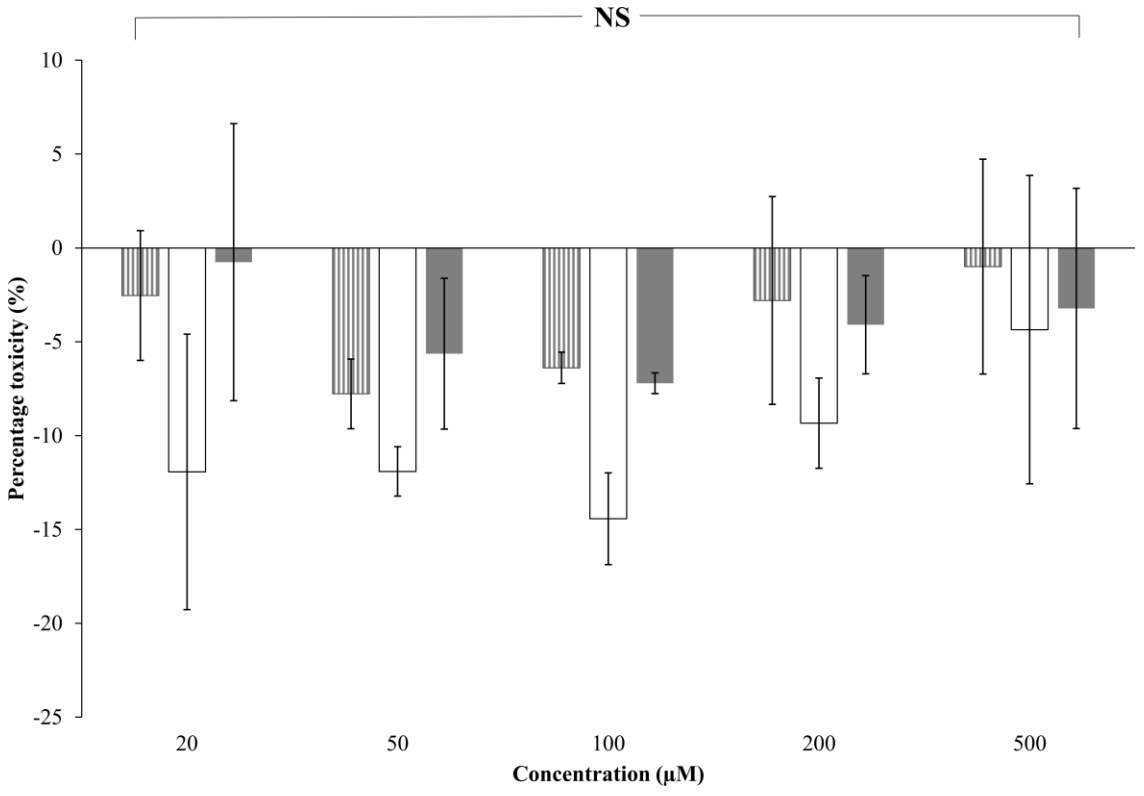

Figure S17. Percentage toxicity of NCTC clone 929 (ATCC CCL 1) cells after 24 hour exposure to varying concentrations of NSAID-peptides. Toxicity is calculated by quantifying LDH release. Key: striped: IbuFFKK, white: IndFFKK, grey: NpxFFKK, ns: no significant difference ($P \geq 0.05$) between the NSAID-peptide and the negative control (PBS).

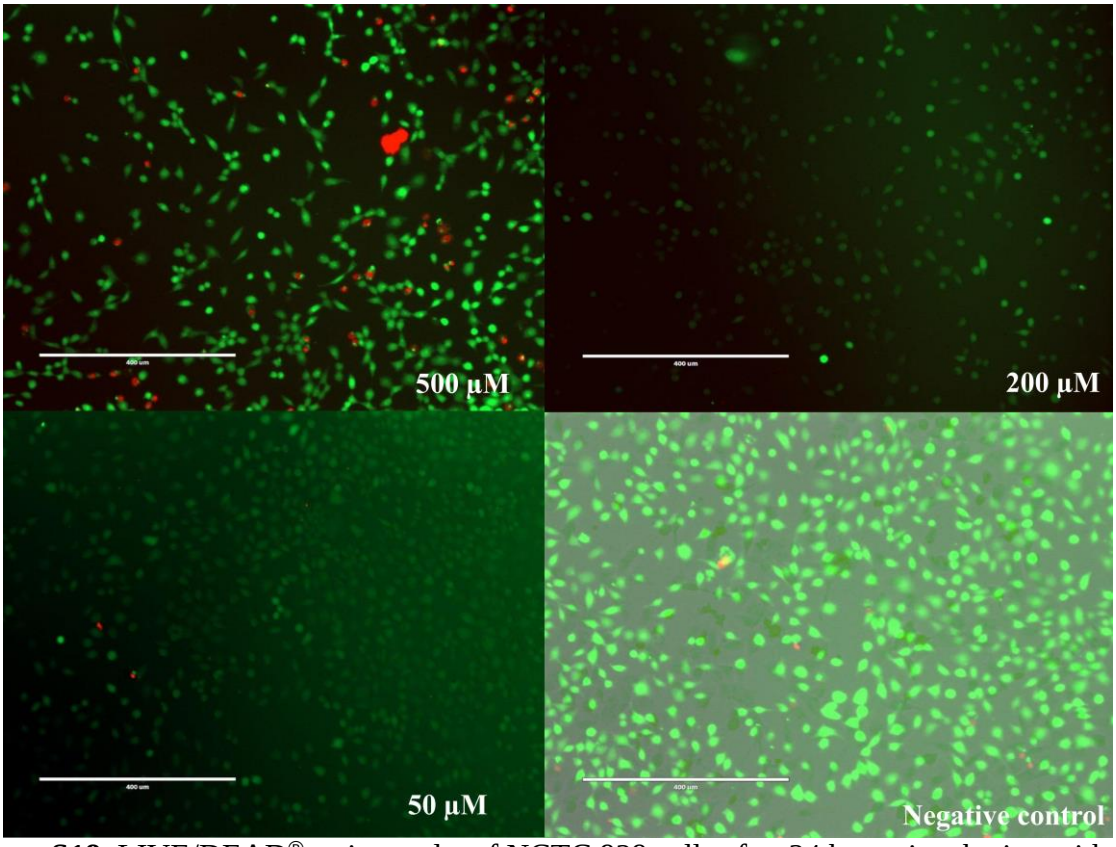

Figure S18. LIVE/DEAD® stain results of NCTC 929 cells after 24 hours incubation with IbuFFKK. Scale bar represents 400 µm, green staining indicates live cells, red staining indicates dead cells.

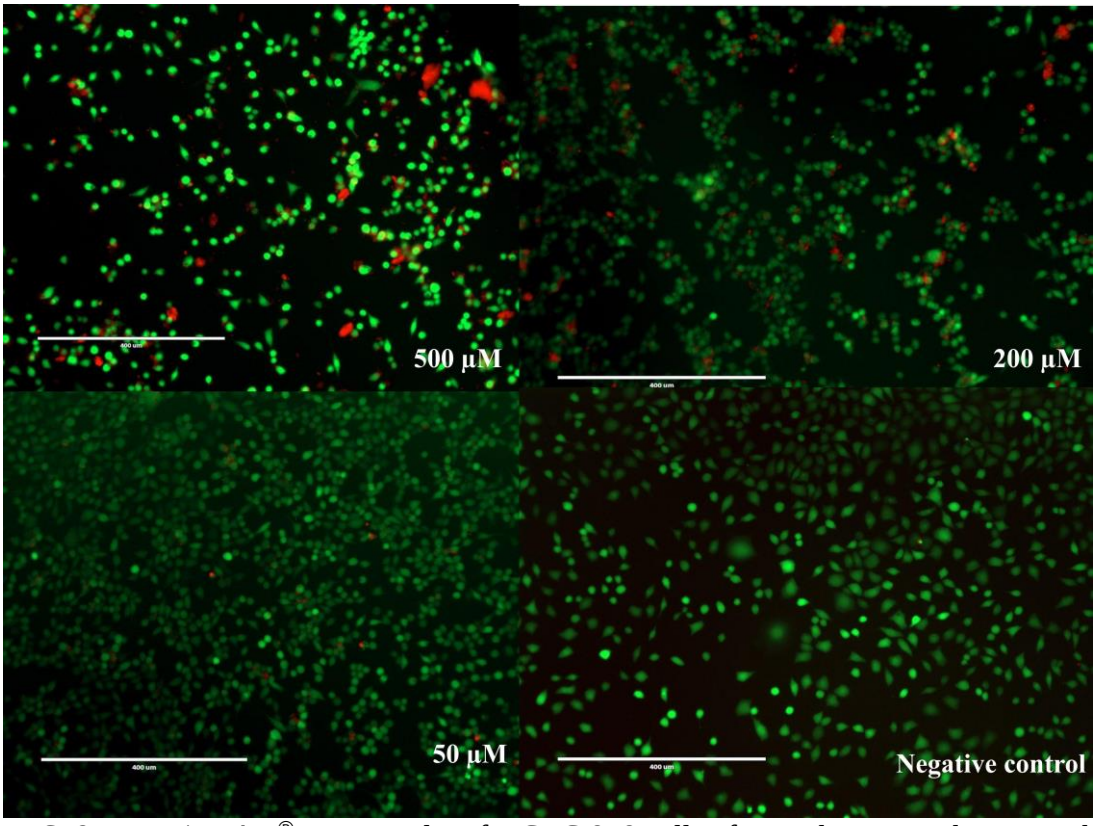

Figure S19. LIVE/DEAD® stain results of NCTC 929 cells after 24 hours incubation with IndFFKK. Scale bar represents 400 µm, green staining indicates live cells, red staining indicates dead cells.

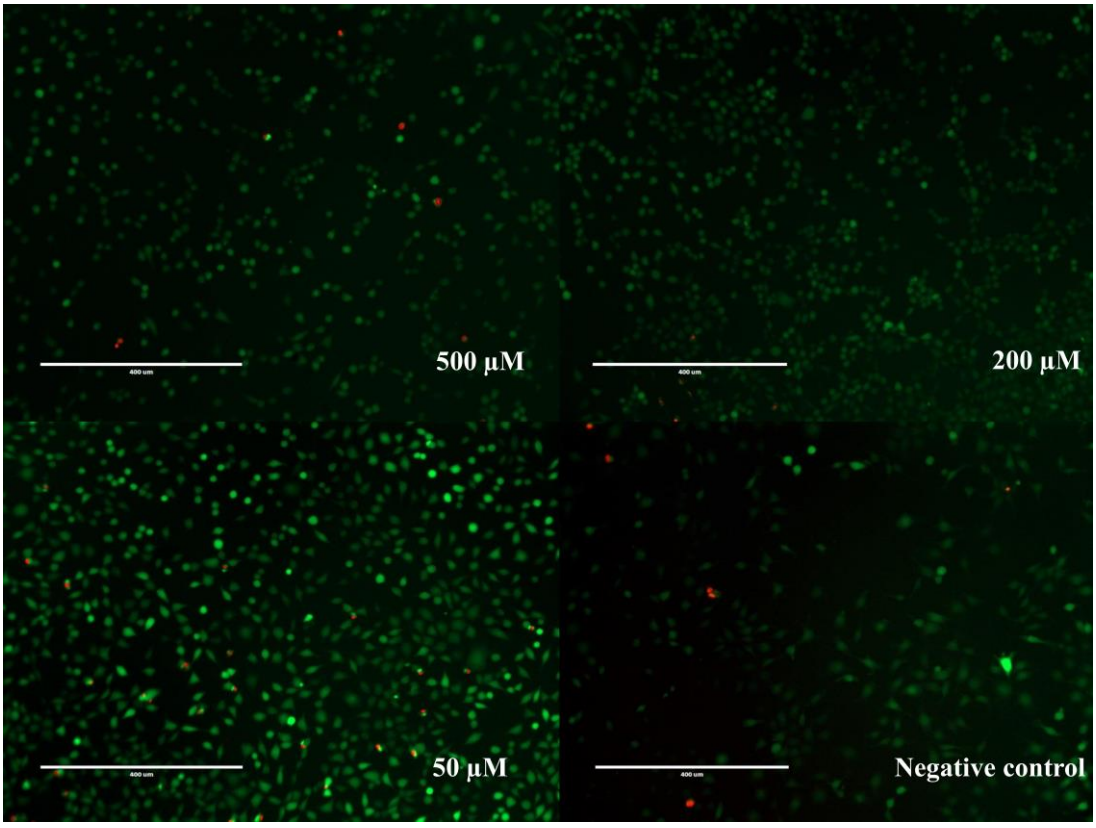

Figure S20. LIVE/DEAD® stain results of NCTC 929 cells after 24 hours incubation with NpxFFKK. Scale bar represents 400 µm, green staining indicates live cells, red staining indicates dead cells.

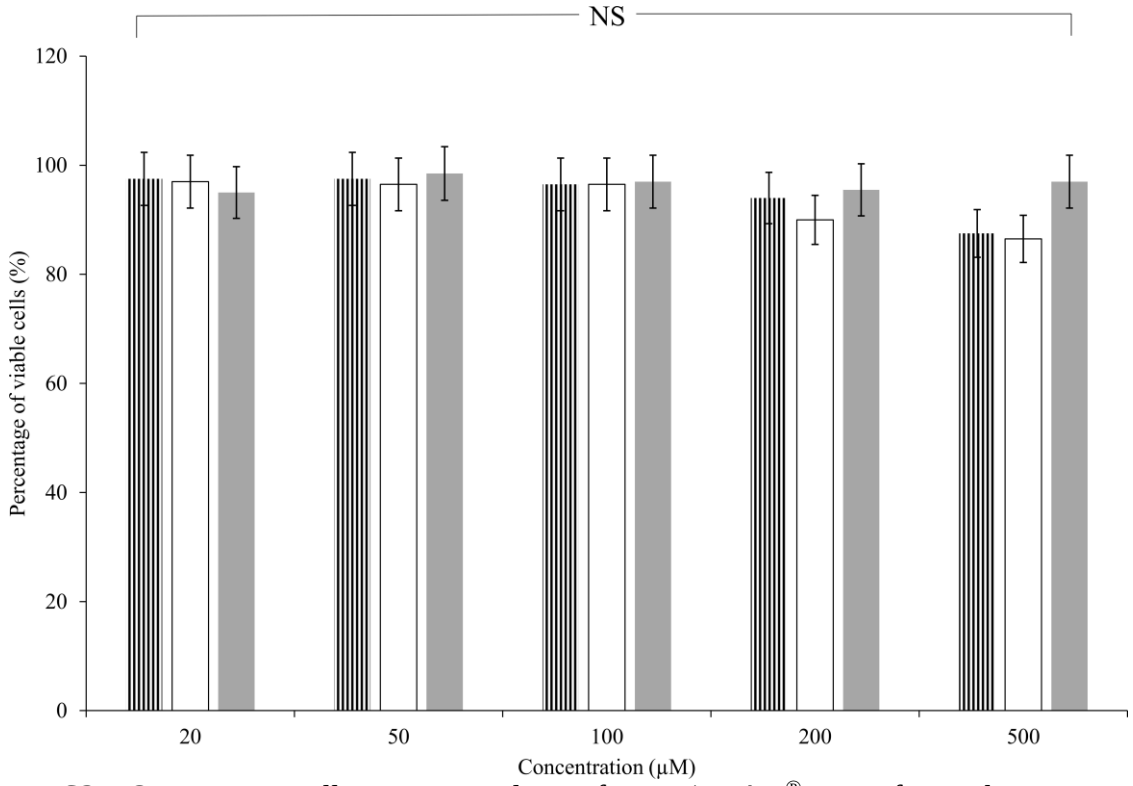

Figure S21. Quantitative cell counting analysis of LIVE/DEAD® stain after 24 hour exposure to varying concentrations of NSAID-peptides. Key: striped: IbuFFKK, white: IndFFKK, grey: NpxFFKK, ns: no significant difference ($P \geq 0.05$) between the NSAID-peptide and the negative control (PBS).